

# POLITECNICO DI TORINO

Master's Degree in Cinema and Media Engineering



Master's Degree Thesis

## Virtual Reality frameworks for non-invasive intracranial explorations

Supervisors

Prof. Francesco P. ANDRIULLI

Prof. Adrien MERLINI

Eng. Davide CONSOLI

Candidate

Eleonora F. MORANA

ACADEMIC YEAR 2020-2021

## Abstract

The objective of this project is to take the first step towards the definition of a model of visual-functional reconstruction of the brain's electrophysiologic activity without having access to patient-specific structural MRI. The proposed approach relies on the combination of electroencephalography (EEG) source localization and machine-learning algorithms for the definition of a standard based on the comparison of discriminating features between brain models.

EEG source imaging (ESI) aims at identifying the areas of the brain responsible for potential variations detected by electrodes placed on the scalp of the patient, and involves the resolution of two fundamental problems: the forward problem and the inverse problem. ESI has several clinical applications ranging from the pre-surgical localization of epileptic seizure-onset zone, or the treatment of psychological disorders via neurofeedback. The localization of the sources occurs by first calculating the electrical potentials resulting from hypothetical neuronal source activity distributions (forward problem), that are then compared with the real data recorded by the EEG to obtain an estimate of the activity that best fit these data (inverse problem). The inverse problem finds its complexity in the ill-posedness of the problem itself. Only by placing reliable *a-priori* constraints is therefore possible to accurately define an electric source, thus solving the inverse problem. The forward problem, instead is well-posed: it is unequivocally determined by the morphologic and electric properties of the patient's head, that can be estimated e.g. by magnetic resonance imaging (MRI).

By obtaining an accurate estimate of the electrical sources it is possible to contextualize them in a three-dimensional model derived from the image processing of a structural MRI. However, the realization of a specific model for a patient for which an ESI is performed is expensive in terms of time, cost and availability of medical equipment. We will therefore build a system capable of sidestepping the need for patient specific MRI head models. We will leverage a structural MRI dataset and build a new algorithm capable of comparing the discriminating brain features derived from the mapping of the scalp of a patient with those related to the three-dimensional models generated by the MRI dataset, and then associate the model that best fits the patient's brain. This will lay the foundations for a new method of EEG source imaging more convenient in economic terms and more reliable in terms of real-time visualization of electrical sources.



# Acknowledgements

Firstly, I would like to thank my supervisors, Francesco Paolo Andriulli and Adrien Merlini. Thank you for your support and for having guided me in every step, from the beginning to the end of this thesis.

A great thanks goes also to the guys of CERL. Thank you for your infinite patience and for all the work you did with me. Thank you Davide, Damiano, Paolo and Alessandro.

I thank my Family, which always believed in this journey as much as me, and inspired me with the dedication and the tenacity they put in everything they do. Thank you for being the best people I could wish to have by my side.

And a thank goes also to my friends, my second family, that are the most precious thing that this city and this University gave me. Thank you for every adventure and for every second you shared with me.

# Table of Contents

<b>List of Figures</b>	VI
<b>Acronyms</b>	IX
<b>1 Introduction</b>	1
<b>2 Theoretical background</b>	3
2.1 Human brain physiology . . . . .	3
2.1.1 The neuron . . . . .	3
2.1.2 Hemishperes and lobes of the brain . . . . .	4
2.2 Neuroimaging . . . . .	5
2.2.1 MRI . . . . .	5
2.3 EEG . . . . .	6
2.4 EEG Source imaging . . . . .	8
2.5 Forward problem . . . . .	8
2.6 Inverse problem . . . . .	10
2.6.1 Non parametric methods . . . . .	11
2.7 Brain Computer Interface . . . . .	13
<b>3 Description of the Project</b>	17
3.1 Hardware . . . . .	17
3.2 Software . . . . .	18
3.3 Neurosurf . . . . .	21
<b>4 3D representation of Brain Models</b>	25
4.1 Head and Brain model reconstruction . . . . .	26
4.2 Tractogram reconstruction . . . . .	27
<b>5 Brain features for brain model selection</b>	37
5.1 Brain Volume . . . . .	38
5.2 Head circumference . . . . .	40

5.3	Body Mass Index . . . . .	40
<b>6</b>	<b>Application-Oriented Model Selection</b>	<b>43</b>
6.1	Focal Seizures and single dipole sources . . . . .	43
6.2	Electrical Potential determination with a reference dipole . . . . .	44
6.3	Model association . . . . .	45
6.4	Computational substitution of brain models . . . . .	47
6.5	Sphere fitting algorithms . . . . .	48
<b>7</b>	<b>Results</b>	<b>51</b>
7.1	Selection of the scalp . . . . .	51
7.2	Internal layers substitution . . . . .	52
7.3	Tests of brain model association . . . . .	54
<b>8</b>	<b>Conclusions and future work</b>	<b>59</b>
<b>A</b>	<b>Subsampling and Clustering</b>	<b>61</b>
<b>B</b>	<b>Sphere-Fitting</b>	<b>65</b>
B.1	Conversion from .MSH to .STL . . . . .	65
B.2	Centering and Scaling . . . . .	65
<b>C</b>	<b>Position of the Dipoles and Conversion of EEG positions</b>	<b>67</b>
C.1	Positions of the Dipoles . . . . .	67
C.2	Conversion of EEG Positions . . . . .	67
	<b>Bibliography</b>	<b>69</b>

# List of Figures

2.1	Graphic description of a spiked neuron. [1]	4
2.2	Subdivision of the brain lobes. [2]	5
2.3	On the left: $T_1$ weighted image, on the right: $T_2$ weighted image. [4]	7
2.4	The BCI cycle. [11]	13
3.1	EEG setup. On the left: g.HiAmp; on the right: EEG cap.	18
3.2	OptiTrack system setup used.	19
3.3	An overview of the Neurosurf User Interface.	22
3.4	Neurosurf's Colormap Gallery.	22
3.5	The electrical activity in Neurosurf, seen with different colormaps.	24
4.1	Image processing in Matlab.	26
4.2	3D model output in Blender 2.9.	27
4.3	MRI image displayed with <code>mrview</code> .	28
4.4	Denoised MRI.	28
4.5	Red: CSF voxels; Green: Grey Matter voxels; Blue: White Matter voxels.	30
4.6	Fiber Orientation Density (FOD) in the 3D space.	30
4.7	Tissue types generated with <code>5ttgen</code> . From the left: grey matter, subcortical grey matter, white matter, cerebrospinal fluid.	31
4.8	Seed boundary.	32
4.9	Streamlines generated with <code>tckgen</code> .	32
4.10	Initial display of the 3D track.	34
4.11	Track after clustering, with random colors.	34
4.12	Different clusters by random colors.	35
5.1	An overview in Blender of the different layers generated with <code>head-reco</code> . From the left: gray matter, scalp, white matter, skull, cerebrospinal fluid.	38
5.2	Correlations between intracranial volume (ICV) and whole-brain ALFF, for the two groups tested. [15]	39

5.3	Relationship between head circumference and brain volume, not grouped by age. [16]	41
5.4	Relationship between head circumference and brain volume, grouped by age. [16]	41
6.1	Calculation of the 10/10 EEG positions based on 4 fiducial points based on the UI 10/10 definition.	45
6.2	Example of a 3D model with its bounding box in the 3D space.	48
7.1	On the left: subject 11. On the right: Scalp of subject 11, subsampled with ratio 0.2 (Blender 2.9).	51
7.2	Scalp of subject012.	52
7.3	From the left: Skull of subject012 and Brain of subject012, subsampled with ratio 0.2.	53
7.4	Scalp of subject012 with its internal layers.	53
7.5	Reference Scalp with the internal layers of subject012.	54
7.6	Plot of the potential detected from the first dipole source (first subject).	56
7.7	Plot of the potential detected from the first dipole source (second subject).	56
7.8	Plot of the potential detected from the second dipole source (first subject).	57
7.9	Plot of the potential detected from the second dipole source (second subject).	57
7.10	Plot of the potential detected from the third dipole source (first subject).	58
7.11	Plot of the potential detected from the third dipole source (second subject).	58



# Acronyms

**ACT**

Anatomically Constrained Tomography

**ADHD**

Attention Deficit Hyperactivity Disorder

**ALFF**

Amplitude of Low Frequency Fluctuations

**ASCII**

American Standard Code for Information Interchange

**BMI**

Body Mass Index

**BCI**

Brain-Computer Interface

**BEM**

Boundary Element Method

**CNS**

Central Nervous System

**CSF**

Cerebro Spinal Fluid

**CT**

Computed Tomography

**DIS**

Distributed Inverse Solution

**dMRI**

diffusion MRI

**DTI**

Diffusion Tensor Imaging

**EEG**

Electroencephalography

**EPSP**

Excitatory Post-Synaptic Potential

**ERP**

Event Related Potentials

**ESI**

EEG Source Imaging

**FEM**

Finite Element Method

**FID**

Free Induction Decay

**FOD**

Fiber Orientation Density

**fMRI**

functional MRI

**FP**

Forward Problem

**GM**

Grey Matter

**WM**

White Matter

**HDRP**

High Definition Render Pipeline

**IP**

Inverse Problem

**IPA**

Isolated Problem Approach

**IPSP**

Inhibitory Post-Synaptic Potential

**IR**

InfraRed

**LORETA**

Low Resolution Electrical Tomography

**MEG**

Magnetoencephalography

**MI**

Motor Imagery

**MNE**

Minimum Norm Estimates

**MRI**

Magnetic Resonance Imaging

**PET**

Positron Emission Tomography

**PSD**

Power Spectral Density

**RAM**

Random Access Memory

**RF**

Radio Frequency

**SDK**

Software Development Kit

**sLORETA**

Standardized Low Resolution Brain Electromagnetic Tomography

**TES**

Transcranial Electric Stimulations

**TMS**

Transcranial Magnetic Stimulations

**SNR**

Signal to Noise Ratio

**UI**

User Interface

**VR**

Virtual Reality

**WMNE**

Weighted Minimum Norm Estimates

# Chapter 1

## Introduction

The complex structure of the brain has been the subject of study and investigation by several scientists in both medical and engineering fields for decades.

With the advent of new technologies, the visualization and observation of the mechanisms that regulate this organ have become increasingly accessible and have led to the creation of various ways to access the data that are regularly produced by the brain itself.

The goal of this work is to discuss and investigate how, by exploiting cutting-edge engineering technologies such as Virtual Reality (VR) and machine learning, basic technologies for the study of electrical signals of the brain such as electroencephalography (EEG) and Neuroimaging technologies such as Magnetic Resonance Imaging (MRI), it is possible to create a three-dimensional representation system capable of visualizing in real time the data produced by our brain in the form of electrical signals.

In particular, from this basis we will delve into the field of EEG Source Imaging, which combines brain structural imaging with brain functional imaging. The former involves all the techniques used to map the anatomy of the brain in its temporal resolution during a mental task, thus without giving information about where the signals detected are generated. The latter involves the techniques used to give information about the metabolic representation of brain structures and their activation based on stimuli. In brief, the aim of EEG Source Imaging is to detect brain stimuli, which can be recorded by an EEG as an electrical potential, and then localize the sources where this stimuli are produced.

EEG Source Imaging involves the resolution of two fundamental problems: the forward problem and the inverse problem. The Forward Problem (FP) consists in the computation of the electrical potential on the scalp generated from the current flow of a single dipole. The Inverse Problem (IP) consists in the localization of the electrical sources by comparing the real potential detected by the EEG with the potential computed solving the IP.

Through electrical signals we are able to have detailed information on neuronal activity, which can be useful in the study of diseases such as epilepsy, cortical or parenchymal lesions of various kinds, or to investigate the secondary nature of more common situations such as headaches. In particular, we will observe how it is possible to perform this representation without necessarily having an MRI for a subject testing our application.

To do this, we will use a large dataset composed of various subjects with related MRIs, then will discuss about various techniques of selection and discrimination to associate which one of these subjects has the characteristics that most closely resemble the brain of a person who in a given moment is wearing our EEG.

The final result will be displayed in our VR application Neurosurf, developed in Unity Engine, whose objective is to give to all its users the opportunity to see neurofeedbacks in real-time without necessarily having an MRI.

# Chapter 2

## Theoretical background

In this chapter we will introduce some theoretical concepts necessary for understanding the main topics of this work. We will discuss basic concepts about human brain physiology (section 2.1) and neuronal activity, then we will introduce the medical technologies we will use in our experiments, i.e. EEG and MRI.

### 2.1 Human brain physiology

The brain is the most complex structure of the human body. It is composed of  $10^{10}$  to  $10^{11}$  cells, called neurons. Each neuron communicates with thousands of other cells that can be either nerve cells, precisely neurons, or muscle cells, sensory cells or endocrine glands. Responsible for this communication are synapses, a structure of interconnections capable of sending chemical or electrical signals. The number of synapses present in the human brain is about  $10^{14}$ .

#### 2.1.1 The neuron

Since we are talking about brain impulses, it is necessary to introduce the concept of neuron. The neuron the main element of the brain, responsible for the transmission of all information that regulates brain activity. Each neuron is in turn composed of three components:

- the soma, which is the body of the neuron and contains the nucleus;
- the axon, a branch of the cell body that plays the key role of transporting nerve signals outside the soma;
- the dendrites, other cellular extensions which receive informations by afferent neurons and direct them to the soma.

Neurons can be defined as electrical devices, which communicate with each other via electrical impulses called action potentials and chemical neurotransmitters.

The channels present in the cell membrane of the neuron allow the flow of positive and negative ions, since the cell membrane itself has its own electrical potential that oscillates between  $-70\text{mV}$  and  $-65\text{mV}$  according to the inputs from the axons of the neuron itself, which inhibit or promote the generation of action potentials [1]. The latter are essentials for communication between neurons, and occur when the electrical potential of the cell membrane reaches  $-50\text{mV}$ , a limit that we call action potential threshold. As shown in fig. 2.1 A neuron that reaches this threshold, graphically speaking, produces a "spike".

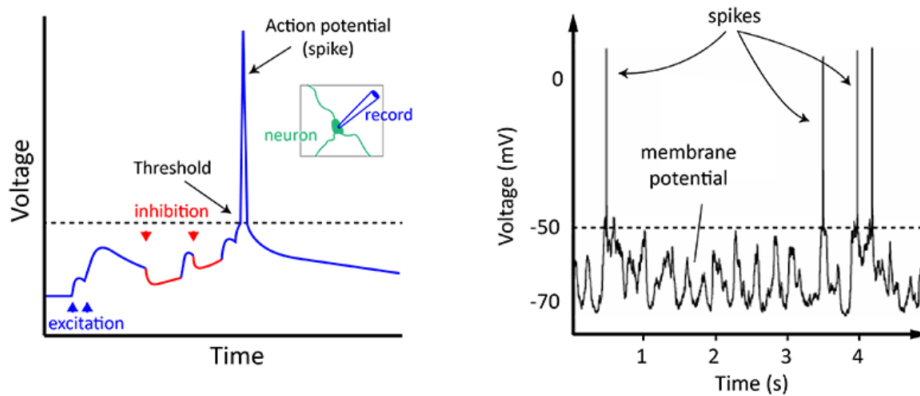


**Figure 2.1:** Graphic description of a spiked neuron. [1]

Neurons communicate with each other through synapses. When an action potential reaches the presynaptic terminal, a neurotransmitter is released into the synaptic cleft, which receptors will attach to a transmitter, and depending on the neurotransmitter released a number of positive or negative ions will cross the cell membrane. In short, synapses convert the electrical signal into a chemical signal in the form of neurotransmitter release, and then bring it back again in the form of an electrical signal.

### 2.1.2 Hemispheres and lobes of the brain

The cerebral cortex is divided into two cerebral hemispheres connected by the corpus callosum [2]. Each one of the hemispheres controls the opposite part of the body (e.g. the left hemisphere controls the right part of the body) and is divided into four lobes: frontal, parietal, temporal and occipital.

As shown in fig. 2.2, the lobes are in turn divided into different areas specialized in various brain functions. For example, in the frontal lobe we will find both

functionalities related to movement, and functionalities related to attention or the ability to speak.

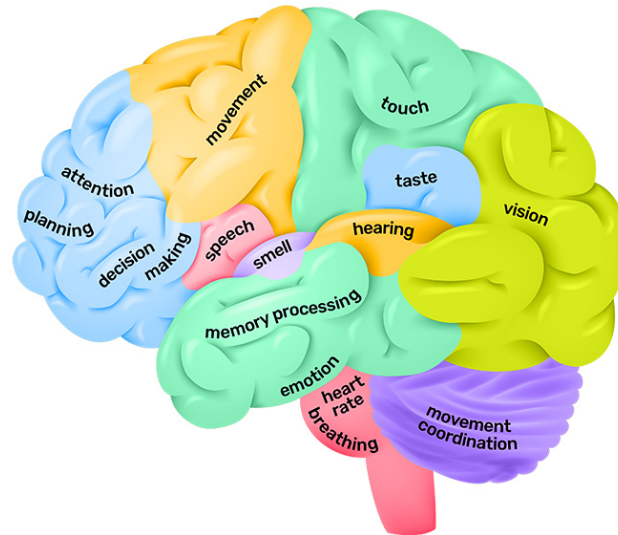


**Figure 2.2:** Subdivision of the brain lobes. [2]

## 2.2 Neuroimaging

With neuroimaging we refer to all medical techniques aimed at mapping the anatomy or physiology of the nervous system (CNS). Neuroimaging techniques are divided into two macrocategories: structural neuroimaging and functional neuroimaging. The former refers to the anatomical representation of brain structures, while the latter refers to the functional, i.e. metabolic representation of brain structures and their activation based on stimuli.

Regarding on structural neuroimaging techniques, among the most widely used are Magnetic Resonance Imaging (MRI) and Computed Tomography (CT). On the other hand, the most widely used functional neuroimaging techniques are functional MRI (fMRI) and Positron Emission Tomography (PET).

### 2.2.1 MRI

Magnetic Resonance Imaging finds its basis in atomic composition and atomic properties. Indeed, all atomic nuclei consist of protons and neutrons, with a net positive charge. Certain atomic nuclei, such as the hydrogen nucleus or the

phosphorus nucleus possess a property known as “spin”. This can be conceived as the nucleus spinning around its own axis [3].

However, the nucleus itself does not spin in the classical meaning, but induces a magnetic moment and generates a local magnetic field with north and south poles. These nuclei can be excited within the static magnetic field ( $\vec{B}_0$ ), that aligns the hydrogen nuclei along its axis, by application of a second radiofrequency (RF) magnetic field ( $\vec{B}_1$ ), applied perpendicular to ( $\vec{B}_0$ ). The RF energy is usually applied in short pulses, each lasting microseconds, and its absorption by the nucleus causes a transition from higher to lower energy levels and vice versa on relaxation. The energy absorbed and emitted induces a voltage that can be detected, amplified and displayed as the “free-induction decay”(FID). In absence of continued RF pulsation, relaxation processes will return the system to thermal equilibrium. Therefore, each nucleus will resonate at a characteristic frequency when placed within the same magnetic field.

In practice, multiple RF pulses are applied to obtain multiple FIDs, which are then averaged to improve the signal-to-noise ratio (SNR). The signal-averaged FID is a time-domain signal. It will be made up of contributions from different nuclei within the environment being studied (e.g. free water and 1H bound to tissue). The signal-averaged FID can be resolved by a mathematical process known as Fourier transformation, into either an image (MRI).

The peculiarity of MRI is that it can provide a weighted image in different sequences, since two types of relaxation are verified, the longitudinal and the transverse relaxation, and they are characterized by two time constants which are, respectively,  $T_1$  and  $T_2$ . Depending on the constant they are weighted to, details will appear differently. In  $T_1$ -weighted images, which we can also call "anatomic sequences" fats will be brighter while fluids, like water, will be darker and vice versa in  $T_2$ -weighted images, since these sequences have opposite gray-scales, as shown in fig. 2.3.

Techniques such MRI are fundamentals in the field of anatomic studies, but they don't have diagnostic implications in the evaluation of functional diseases (unless they are secondary to organic lesions e.g. secondary epilepsy). For the evaluation of functional neuronal activity, the gold standard examination is the Electroencephalogram (EEG).

## 2.3 EEG

Electroencephalography (EEG) is a non-invasive technique based on the principle that neurons are interconnected between each other by dendrites, which connect to form synapses. Therefore, neuronal communication occurs through these electrical synapses. When a large group of neurons produces electrical activity, a current

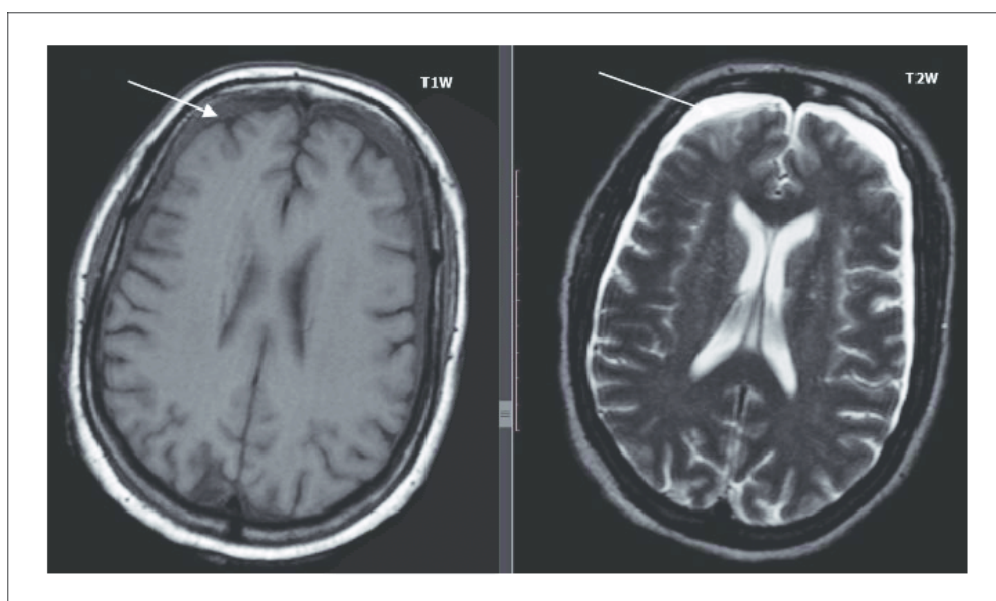


**Figure 2.3:** On the left:  $T_1$  weighted image, on the right:  $T_2$  weighted image. [4]

flow is generated and it causes an electric field and a potential field inside the human head. When these fields reach the head surface, the electrodes can detect the electrical potential generating the EEG itself.

The activity recorded by the EEG concerns the events inside a neuron when a synapses takes place. Indeed, when a neuron is active, it secretes a neurotransmitter at the synaptical side, where the dendrites are located. A postsynaptic neuron has a large number of receptors which make contact whit the neurotransmitter secreted, changing the permeability of the cell membrane. Depending on the neurotransmitter, two kinds of events can happen [5].

At rest, the cell membrane is characterized by a polarization of about  $-70\text{mV}$  due to unequal distribution of  $\text{Na}^+$ ,  $\text{K}^+$  and  $\text{Cl}^-$  ions across it. If the receptor make contact with a neurotransmitter which let the neuron signals proliferate, an influx of positive ions will change the permeability of the cell membrane with a consequent depolarization of the intra-cellular space, from  $-70\text{mV}$  to  $-40\text{mV}$ . We can call this depolarization as Excitatory Postsynaptic Potential (EPSP). If the receptor make contact with a neurotransmitter which stops the proliferation of neuron signals, the consequence will be an outflow of positive ions, causing an hyperpolarization called Inhibitory Postsynaptic Potential (IPSP).

As we mentioned in section 2.1.1, when an intracellular depolarization reaches a threshold, an action potential is generated and it propagates to other neurons. The electrodes of the EEG can't detect the action potentials since they have a small time course (about  $0.3\text{ ms}$ ). On the other hand, the postsynaptic potentials have

a larger time course which enables simultaneous activity of neighboring neurons. These potentials generate the extracellular potential field detected by the EEG. This current can be modeled by Poisson's equation.

Electroencephalography provides information that primarily concerns disturbances of function rather than structure, such as epilepsy diseases [6]. However, most EEG applications fail to capitalize on all of the data's available information, particularly that concerning the location of active sources in the brain, since this technique lacks of detailing the spatial resolution of the brain activity.

To investigate the spatial properties of brain activity, we must introduce the EEG Source Imaging (ESI), which simultaneously details the temporal and spatial dimensions of brain activity [7].

## 2.4 EEG Source imaging

The pure electroencephalography itself can't give accurate information about the spatial dimension of the brain activity.

EEG Source imaging concerns the field of studies which investigates the localization of the electrical sources which generate the current flow detected by an electroencephalogram, which means also giving a functional feedback for the brain. Indeed, functional neuroimaging has the aim of localizing the different modules of the functional network implicated in a given mental task, but the principal functional techniques such as functional Magnetic Resonance (fMRI) and Positron Emission Tomography (PET) are not accurate to answer the question of when the involved brain areas become active during the mental task. EEG source imaging finds its applications in several science fields such as neurology, psychiatry and psychopharmacology and all the sciences which investigate the temporal aspects of information processing by analyzing event related potentials (ERP). The main clinical application concerns the localization of epileptic foci [7].

EEG source localization consists on solving two fundamental problems: the forward problem (FP) and the inverse problem (IP).

## 2.5 Forward problem

The forward problem consists in the computation of the potential at the electrodes starting from a given electrical source of a single dipole and its solution is needed to solve the inverse problem [5].

The electrical activity of groups of neurons can be modeled by means of current dipoles with moment  $\mathbf{d}$ , characterized by a magnitude  $d = \|\mathbf{d}\|$  and an orientation  $\mathbf{e}_d$ . By solving the Poisson equation we can calculate  $g(\mathbf{r}, \mathbf{r}_{dip}, \mathbf{d})$ , the potential

at an electrode having a position vector  $\mathbf{r}$  due to a single dipole with moment  $\mathbf{d}$  located in  $\mathbf{r}_{dip}$ , considering the different configurations of  $\mathbf{r}_{dip}$  and  $\mathbf{d}$ .

If we consider multiple dipole sources, according to the superposition principle, the potential at an electrode is

$$V(\mathbf{r}) = \sum_i g(\mathbf{r}, \mathbf{r}_{dip_i}, \mathbf{d}_i) = \sum_i g(\mathbf{r}, \mathbf{r}_{dip_i}, \mathbf{e}_{d_i}) d_i. \quad (2.1)$$

In practice, the difference between an electrode and a reference is calculated. The reference could be another electrode or an average reference. For  $N$  and  $p$  dipoles we can imagine the potential  $V$  as a column vector resulting by the product between the matrix which describes the different values of  $g(\mathbf{r}, \mathbf{r}_{dip}, \mathbf{d})$  depending on the value of  $N$  and the dipole  $p$  and the column vector of the moment  $d$ . Then, given  $p$  dipoles,  $N$  electrodes, and considering  $T$  time samples, the forward problem can be expressed as

$$\mathbf{V} = \mathbf{GD} + \mathbf{n} \quad (2.2)$$

where  $\mathbf{V}$  indicates the  $N$ -by- $T$  matrix of the potentials measured at different times at the electrodes positions,  $\mathbf{G}$  indicates the  $N$ -by- $p$  gain matrix,  $\mathbf{D}$  indicates the  $p$ -by- $T$  matrix of the magnitudes of the dipoles at different time instants, and  $\mathbf{n}$  is a noise distribution, in particular a Gaussian distribution whit zero mean and variable standard deviation. This component added to take into account the possible perturbations of the EEG measurements, even if it does not represent accurately the real noise which can depend on different factors like the patient's pathology or the measurement set up. The gain matrix is also called "lead-field matrix" and it represents the physical properties of the head.

Solving the forward problem is essential to approach with the inverse problem, since the estimated potential  $V$  is necessary in order to work back and localize the electrical sources. One of the most used technique to solve the forward problem and calculate the surface potentials is the Boundary Element Method (BEM). It is a low computational need technique and for this reason it is widely used. It consists on calculating the potentials generated by current sources located in a picewise homogeneous volume conductor [5].

It is based on the fact that a head model is generally composed of 3 surfaces: brain-skull interface, skull-scalp interface and the outer surface, and the region between these surfaces are homogeneous and isotropic conducting. This method provides a solution to a volume problem by calculating the potential values at the interfaces and boundary of the volume induced by a given current source. The equations which describe this approach can be resumed into a set of linear equations:

$$\mathbf{V} = \mathbf{BV} + \mathbf{V}'_0 \quad (2.3)$$

where  $\mathbf{V}$  and  $\mathbf{V}'_0$  indicate the column vectors denoting at every node the wanted potential and the potential value in an infinite homogeneous medium due to a source [5],  $\mathbf{B}$  is a matrix whose values depend on the geometry of the surfaces and the connectivity of each region. The determination of the values of  $\mathbf{B}$  has a high computational cost. Moreover, using this matrix the equation has no unique solution and this means that  $\mathbf{B}$  must be replaced by

$$\mathbf{C} = \mathbf{B} - \frac{1}{N} \mathbf{e} \mathbf{e}^T \quad (2.4)$$

where  $e$  is a vector with all is  $N$  components, that are all the unknowns, equal to one. The previous equation become

$$\mathbf{V} = \mathbf{C} \mathbf{V} + \mathbf{V}'_0 \quad (2.5)$$

and possesses a unique solution that is also a solution of the original one. Moreover, in order to reduce the errors that could be generated considering the difference between the conductivity of the brain and the conductivity of the skull we can follow the Isolated Problem Approach (IPA) and rewrite  $V$  as

$$\mathbf{V}'(\mathbf{r}) = \mathbf{V}'(\mathbf{r}) + \mathbf{V}''(\mathbf{r}) \quad (2.6)$$

where  $V''$  is defined as the potential on the surface when the head is a homogeneous brain region, thus omitting the skull and the scalp compartments [5].  $V'$  is the correction term.

Another widely used technique to solve the forward problem is the Finite Element Method (FEM) which solves the Poisson's equation in a realistic head model. However, its computational cost is very intensive.

## 2.6 Inverse problem

Our main objective is to illustrate how to approach with the Inverse Problem (IP). Solving the Inverse Problem means identifying the electrical sources that generate the current flow detected by the EEG, starting from the results obtained by solving the Forward Problem.

The complexity of solving the IP lays in the ambiguity of the problem itself, since we can't identify the source as a single dipole and due to this the equation which describes the problem has infinite solutions. Indeed, while in the Forward Problem we analyzed the current flow generated from a single dipole with a specific behavior, in the case of IP we work back from the potential  $V$  detected by the EEG that we can't consider as a potential coming from a single source but from a higher amount of electrical sources. The only way to solve this problem is to apply some reliable constraints which can lead to an accurate result [8].

As we showed in section 2.5, the neural activity can be modeled by currents. Considering  $N$  electrodes with position vector  $r$ ,  $p$  dipoles with position vector  $r_{dip}$  and moment  $d$ ,  $T$  instants, we obtained the equation

$$\mathbf{V} = \mathbf{GD} + \mathbf{n} \quad (2.7)$$

Where  $V$  is the column vector of the potentials at different times,  $G$  is the lead-field matrix,  $D$  is the matrix describing the dipole moments at different times and  $n$  is the added Gaussian noise which could derive from several factors. However, we must consider that for the Inverse Problem  $p \gg N$  and the system becomes unstable and the solution is non-unique.

Starting from eq. (2.7), the aim is to estimate the matrix  $D$  knowing  $V$  from the EEG recordings and  $G$  from the Forward Problem. Among the approaches used to solve the Inverse Problem, we find two main methods:

- non parametric methods, that we also can call Distributed Source Model, Distributed Inverse Solutions (DIS) or Imaging methods. The use of these method leads to a linear problem.
- parametric methods. The use of these methods leads to a non-linear problem.

We will focus on non-parametric methods.

### 2.6.1 Non parametric methods

As we mentioned in section 2.4, dipole sources are assumed as intracellular currents located in the dendritic trunks which are oriented to the cortical surface.

In this model we consider several dipoles with fixed locations and possibly fixed orientation. So  $\mathbf{r}_{dip_i}$  and  $\mathbf{e}_i$  are respectively determined and possibly determined a-priori. If these dipoles have a fixed orientation it means that they are normally aligned and then the amplitudes and direction can be estimated. For this reason we can define this a linear problem. Among these approaches we can find:

- Bayesian methods, based on the probabilistic approach to find a probability distribution of solutions;
- The Backus-Gilbert method, which finds the approximate inverse operator  $\mathbf{T}$  of  $\mathbf{G}$  to estimate the closest current density to the real current density, using real EEG data;
- The weighted resolution optimization, an extension of the previous Backus-Gilbert;

the Bayesian methods, which focus on finding a probability distribution of solutions instead of a single one. We will focus on the Bayesian methods, in particular in the Low resolution electrical tomography (LORETA) and in the Standardized low resolution brain electrical tomography (sLORETA).

### Low resolution electrical tomography (LORETA)

Low resolution electrical tomography is a non-parametric method which combines the lead-field normalization with the Laplacian operator. It based on the maximum smoothness of the solution, starting from the constraint of smoothly distributed sources. LORETA analyzes all the sources, from the deeper ones to the most superficial ones and normalizes the columns of the lead-field matrix  $\mathbf{G}$  to give these sources the same opportunity of being reconstructed.

$$\hat{\mathbf{G}}_{\text{LOR}} = (\mathbf{G}^T \mathbf{G} + \alpha \mathbf{B} \Delta^T \Delta \mathbf{B})^{-1} \mathbf{G}^T \mathbf{M} \quad (2.8)$$

Where  $\mathbf{B}$  is a diagonal matrix for the column normalization of  $\mathbf{G}$ .

According to the aim of our work, this method is important since it was analyzed and compared among four other inverse methods (minimum norm, weighted minimum norm, Backus-Gilbert, weighted resolution optimization) thus resulting the best one in the localization of the sources in 3D space.

### Standardized low resolution brain electromagnetic tomography

Standardized low resolution brain electromagnetic tomography (sLORETA) is a method which focuses on the source localization based on images of standardized current density. [9] Despite the name, it is different from LORETA since it does not use the Laplacian operator and the concept itself is quite different [8]. It uses the current density  $\hat{\mathbf{G}}_{\text{MNE}}$  estimated by another non-parametric method, Minimum Norm Estimate (MNE). With sLORETA the variance of this current density is estimated by referring to the actual source variance, while its variation is estimated by referring to the noisy measurements. Thus  $\hat{\mathbf{G}}_{\text{MNE}}$  becomes standardized. The method can be described by the following equation:

$$\hat{\mathbf{D}}_{\text{MNE},l}^T \{[S_{\hat{D}}]_{ll}\}^{-1} \hat{\mathbf{D}}_{\text{MNE},l} \quad (2.9)$$

Where  $\hat{\mathbf{D}}_{\text{MNE},l}^T$  is the current estimate at the  $l$ th voxel given by MNE and  $[S_{\hat{D}}]_{ll}$  is the  $l$ th diagonal block of the resolution matrix  $S_{\hat{D}}$  [8]. sLORETA selects the source with maximum normalized power as the centre point for spatial refinement in the next iteration, where the next decimation is applied. It solves the IP giving a smooth solution.

sLORETA has zero error localization on single sources, since the maximum of the current density power estimate corresponds to the dipole location. It has

also good results in noisy simulations, since it produces results with the lowest localization errors and least number of ghost sources.

## 2.7 Brain Computer Interface

Brain-computer interface (BCI) is a method of communication based on neural activity generated by the brain and is independent of its normal output pathways of peripheral nerves and muscles [10].

The BCI system is always subject to the conditions in which it operates. Therefore, an operating environment is defined and it indicates the physical location and the surrounding objects in which the system is used. It involves physical boundaries, temperature, terrain conditions, external noises. The system must be able to endure the changing conditions and adapt to them.

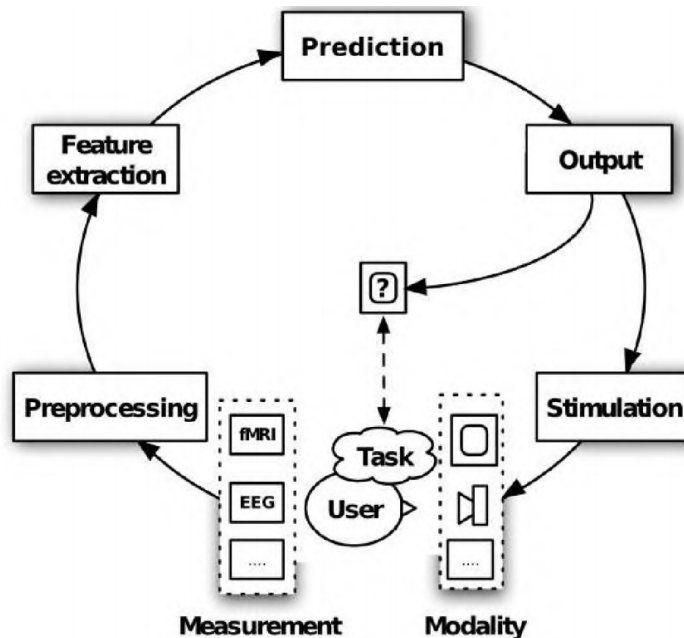


Figure 2.4: The BCI cycle. [11]

An user is defined as the entity which intentionally alters his brain state (here we exclude involuntary changes of the brain state, such as seizures) to give an input to the BCI system in the shape of control signals.

The cycle of a BCI system can be resumed in 6 phases (fig. 2.4):

- Task and stimuli of the user;

- Measurement;
- Preprocessing of the detected data;
- Feature extraction;
- Prediction;
- Output.

### **Task and stimuli**

To start the BCI cycle, a mental effort of the user is required to produce a change of the brain state to be detected. The ideal BCI mental task should be produced without a great effort to prevent fatigue, so that large brain signal could be generated. This situation is actually ideal, since the effort required to produce sufficiently large signal is high and makes the user fatigued. The first device developed in the field of BCI used voluntarily generated brain activity, thus excluding involuntary changes of the brain state (seizures).

Several recent approaches have focused on instructed cognitive tasks, which range from perceptual tasks, such as selective attention, via imagery of perception or movement, to higher level mental tasks such as associating concepts, reasoning and mental arithmetic. Among imagery tasks, Motor Imagery (MI) is currently the most popular.

### **Measurement**

The measurement techniques of BCI can be divided into invasive techniques and non-invasive techniques. Non-invasive electroencephalography (EEG) and magnetoencephalography (MEG) reflect the neuronal activity generated by dipole sources. The temporal resolution of EEG and MEG to measure changes in neuronal activity is good but the spatial resolution to determine the precise position of active sources in the brain is poor. On the other hand, Magnetic Resonance Imaging (MRI) has optimal results in spatial resolution but lacks of temporal resolution.

### **Preprocessing and feature extraction**

The data detected by the measurement devices must be preprocessed so that the signal-to-noise-ratio (SNR) is minimized and produces correct brain state identifications [11]. The most common techniques of preprocessing are artifact detection, spectral filtering and spatial filtering. Artifact detection detects all the signals which are not produced by neural activity and then attempts to remove them from the trial data. Spectral filtering is used to remove noise signals and spatial

filtering linearly combines signals from multiple electrodes to focus on activity at a particular location in the brain.

Feature extraction is based on characterizing the signals preprocessed. The objective in these two phase is to make the raw signals readable for the prediction phase.

### **Prediction**

This phase is concerned with Machine Learning algorithms. If the output is continuous, we deal with a regression problem and if the output is discrete we deal with a classification problem [11]. The prediction is the main phase of the BCI cycle and its problems consist on the choice of a proper feature selection, in order to have a good performance on the on-line state estimation and on the adaption of the BCI system when the brain state changes during the iteration.

### **Output**

The BCI output closes the BCI cycle. It generates information for controlling an output device which can be a computer application or a physical device like a wheelchair [11]. The output gives the user a feedback about the predicted intention that was produced by the mental task of the user. Output can take a wide range of output modalities, such as text, auditory output or graphica representations of brain activity for neurofeedback, such as in our work.



# Chapter 3

## Description of the Project

In this chapter we will have an overview of all the assets and devices used to develop the application, from the hardware components to the software for the data processing.

### 3.1 Hardware

The hardware components used for the realization of the application Neurosurf characterize a fundamental part of the project. In particular, to achieve the data detection and the volume tracking of the user's scalp were used:

- Electroencephalograph;
- OptiTrack system.

#### EEG

Two systems for EEG were used:

- g.HiAmp, a high-performance biosignal amplifier with 256 channels for invasive and non-invasive measurements. The 256 channels can be analyzed in real-time.
- g.Nautilus, which is a wearable EEG headset to record brain activity in medical and clinical environments. The different electrode strands hold 8/16/32 EEG electrodes.

Both use active electrodes and wet measurements.

Figure 3.1 shows the EEG setting used for g.HiAmp and the cap on which the electrodes for the EEG are positioned.

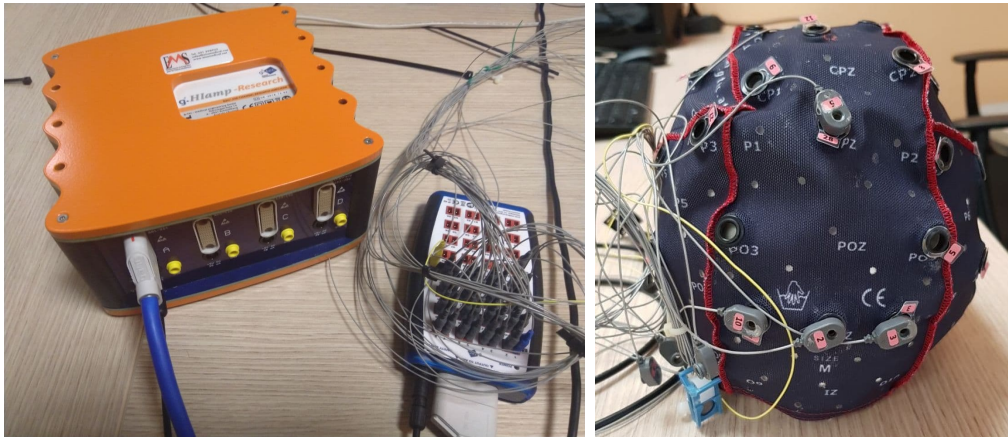


**Figure 3.1:** EEG setup. On the left: g.HiAmp; on the right: EEG cap.

## OptiTrack

OptiTrack is a motion capture system. It works by placing multiple markers on a defined volume and executes a sub-millimetre tracking of these markers, with a frequency up to  $240Hz$ .

In our asset, the tracking was realized with 8 OptiTrack Prime 13W cameras with  $1.3MP$  resolution, a vertical FoV of  $58^\circ$  and a horizontal FoV of  $70^\circ$ . These cameras are placed over a  $5m \times 5m \times 3m$  metallic cage (see fig. 3.2) and they work by detecting the positions of the reflections in the infrared (IR) spectrum. Then the 3D locations of the markers are computed and the mesh of the tracked volume is generated.

## 3.2 Software

The software used to process the data and to visualize our outputs is described in the following sections.

### Unity Engine

Unity Engine is a cross-platform game engine developed by Unity Technologies. It is the leading platform for creating 2D, 3D and VR interactive/real-time content. The project in Unity is organized in scenes, which include an interface to interact with the possible commands and the game itself, where the user can experience the intracranial exploration through the GameObjects present in the scene. The visualization of the scenes while using an Unity application is made possible by setting a Camera. Also the User Interface (UI) is a GameObject called Canvas, where



**Figure 3.2:** OptiTrack system setup used.

all the elements of the UI should be placed. The interaction with GameObjects is managed by the scripts which describe and regulate their behavior.

The Unity application can be used as an executable file after having built the project, assuming that all the scripts that regulate the world have no errors.

### **MatLab and Simulink**

MATLAB, an abbreviation of "matrix laboratory" is a programming language and numeric computing environment developed by MathWorks. MATLAB allows matrix manipulations, plotting of functions and data, implementation of algorithms, creation of user interfaces, and interfacing with programs written in other languages.

Simulink is a MATLAB-based graphical programming environment for modeling, simulating and analyzing multidomain dynamical systems. Its primary interface is a graphical block diagramming tool and a customizable set of block libraries. Simulink is widely used in automatic control and digital signal processing for multidomain simulation and model-based design.

## **SimNIBS**

SimNIBS is a free and open source software package for the Simulation of Non-Invasive Brain Stimulation. It allows for realistic calculations of the electric field induced by transcranial magnetic stimulation (TMS) and transcranial electric stimulation (TES).

We used this software to process the MRIs collected, through the command `headreco`. `Headreco` reconstructs a tetrahedral head mesh from T1- and T2-weighted structural MR images. All the head meshes reconstructed in our dataset were processed with `headreco`.

## **MRtrix3**

MRtrix3 provides a set of tools to perform various types of diffusion MRI analyses, from various forms of tractography through to next-generation group-level analyses. It is developed and maintained by a team of experts in the field, fostering an active community of users from diverse backgrounds. It was used to generate the streamlines, starting from T1-weighted MRI and diffusion tensor.

## **Gmsh**

Gmsh is an open source 3D finite element mesh generator with a built-in CAD engine and post-processor. Gmsh is built around four modules: geometry, mesh, solver and post-processing. The specification of any input to these modules is done either interactively using the graphical user interface, in ASCII text files using Gmsh's own scripting language (.geo files), or using the C++, C, Python or Julia Application Programming Interface (API) [12].

We used Gmsh either for the visualization of the brain models generated and for the simulations performed to place the electrodes and calculate the lead-field matrices.

## **Blender**

Blender is an open source environment which deals with 3D modeling, animation, rigging, compositing and video editing. We used this software to visualize and manipulate the 3D models generated as an output from processed MRIs. In particular, we used Blender to apply modifiers in order to subsample the meshes generated with Simnibs and to separate and manipulate the various layers that were given as a unique output.

## 3.3 Neurosurf

Neurosurf is an interactive VR application developed and built in Unity Engine. The application allows an user to experience an intracranial exploration based on the recording of his electrical activity, which can be visualized in real-time.

As we mentioned in section 3.1, the electrical activity is recorded with an EEG. The main problem of this technique is due of its lack of spatial resolution, which is on the other hand a characteristic of Magnetic Resonance Imaging. The goal of Neurosurf is to combine the temporal resolution of the EEG with the spatial resolution of MRI, giving the user the opportunity of a structural-functional analysis of his brain. It could help in the study of functional diseases such as ADHD, schizophrenia or epilepsy.

The EEG measurements (pre-recorded or real-time) are processed with a Python script, which sends the data to the application and the elements in the scene become active. These elements are the different layers which compose a human head. Neurosurf receives the data that are linked to some of these layers (e.g. brain, fibers) and their activation is represented by flashing lights and colors belonging to a specific colormap selected by the user. The areas which become active correspond to the electrical sources localized. In particular, the elements in the scene are:

- User Interface (UI);
- Scalp;
- Skull;
- Brain;
- Fibers;
- Game controller, lights and Camera.

### User Interface

The Neurosurf environment starts, pauses and stops with the User Interface's Main Menu. The UI also offers the access to the Colormap Gallery fig. 3.4, where the user selects the colormap to visualize the electrical activity, and to the Opacity Settings where an user can set the opacity of the different layers in the scene.

### Scalp

The scalp is the most external layer which corresponds to the surface where the electrodes are placed. Thus, here the electrical potential  $V$  is detected. The scalp

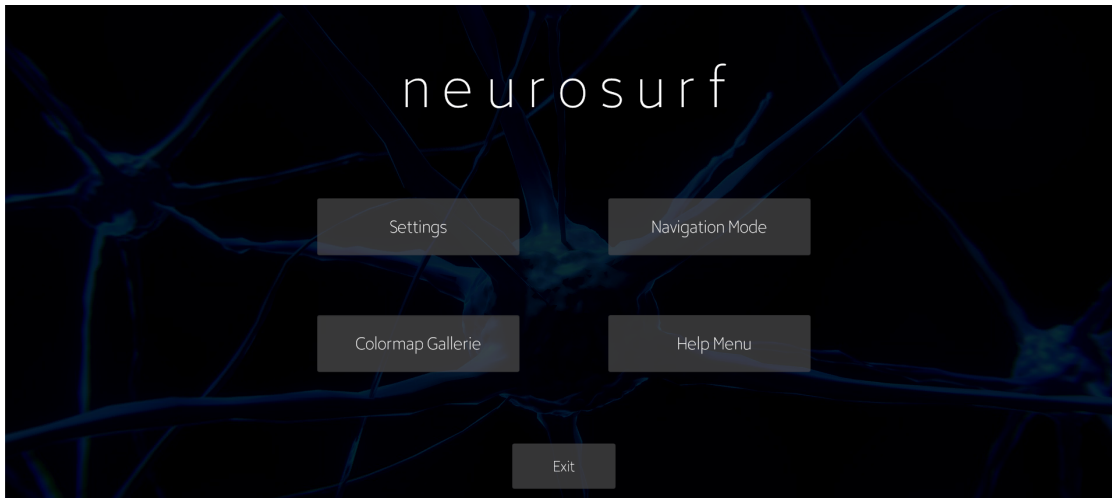


**Figure 3.3:** An overview of the Neurosurf User Interface.

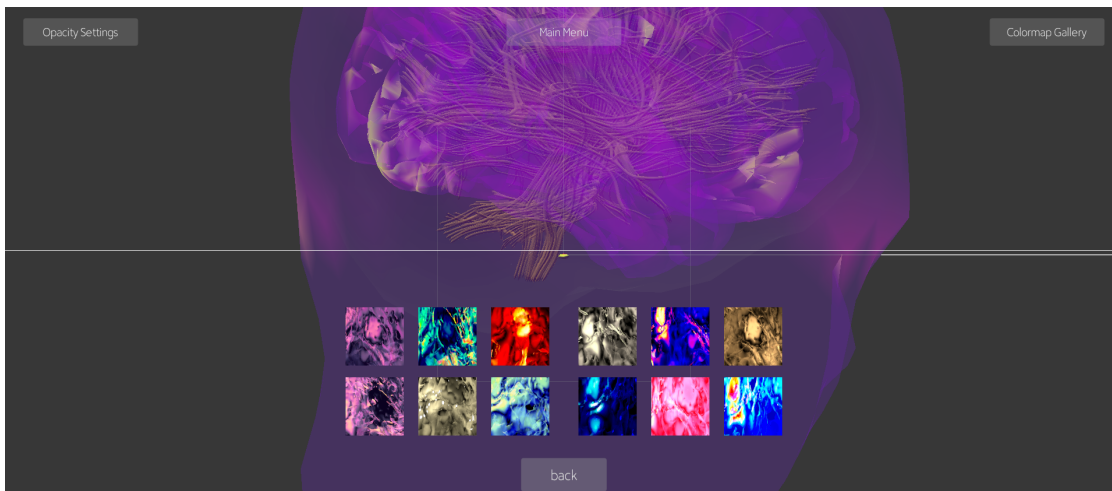


**Figure 3.4:** Neurosurf's Colormap Gallery.

is a 3D mesh generated from the processing of MRI images, and in our work is the unique layer which remain fixed. The most internal layers change according to the brain model selection, that we will discuss in the following chapters.

### Skull

The skull is the intermediate layer which separate the Scalp from the internal layers, Brain and Fibers. It is a kind of "obstacle" for the potential detection, since its conductivity is significantly lower than the conductivity of the brain. Therefore, this causes an amplification of the numerical errors in the calculation of the electric

potential.

## **Brain**

The brain is the most important element in the scene. It is also generated with MRI image processing and it is a complex and very defined 3D mesh: without any kind of subsampling, its vertex-count reaches up to one million. In the brain, the electrical sources are localized by solving the Inverse Problem (section 2.6) of EEG Source Imaging.

## **Fibers**

While Scalp, Skull and Fibers are generated together with the MRI image processing, the Fibers require a more complex pipeline to be reconstructed. We will talk about this pipeline in the following chapter (section 4.2).

The fibers are the most internal layer of the whole mesh present in the scene. They connect the cortical areas of the brain where the impulses are visualized.

## **Game Controller, Lights and Camera**

The game controller is a kind of 'remote' used to interact with the VR system. The camera object is necessary to determine what can be seen by the user and how it appears in the viewport.

The lights are GameObject which produce light. They are essential in order to see the environment. Indeed, even if the camera is present it is impossible to see the scene without some lights.

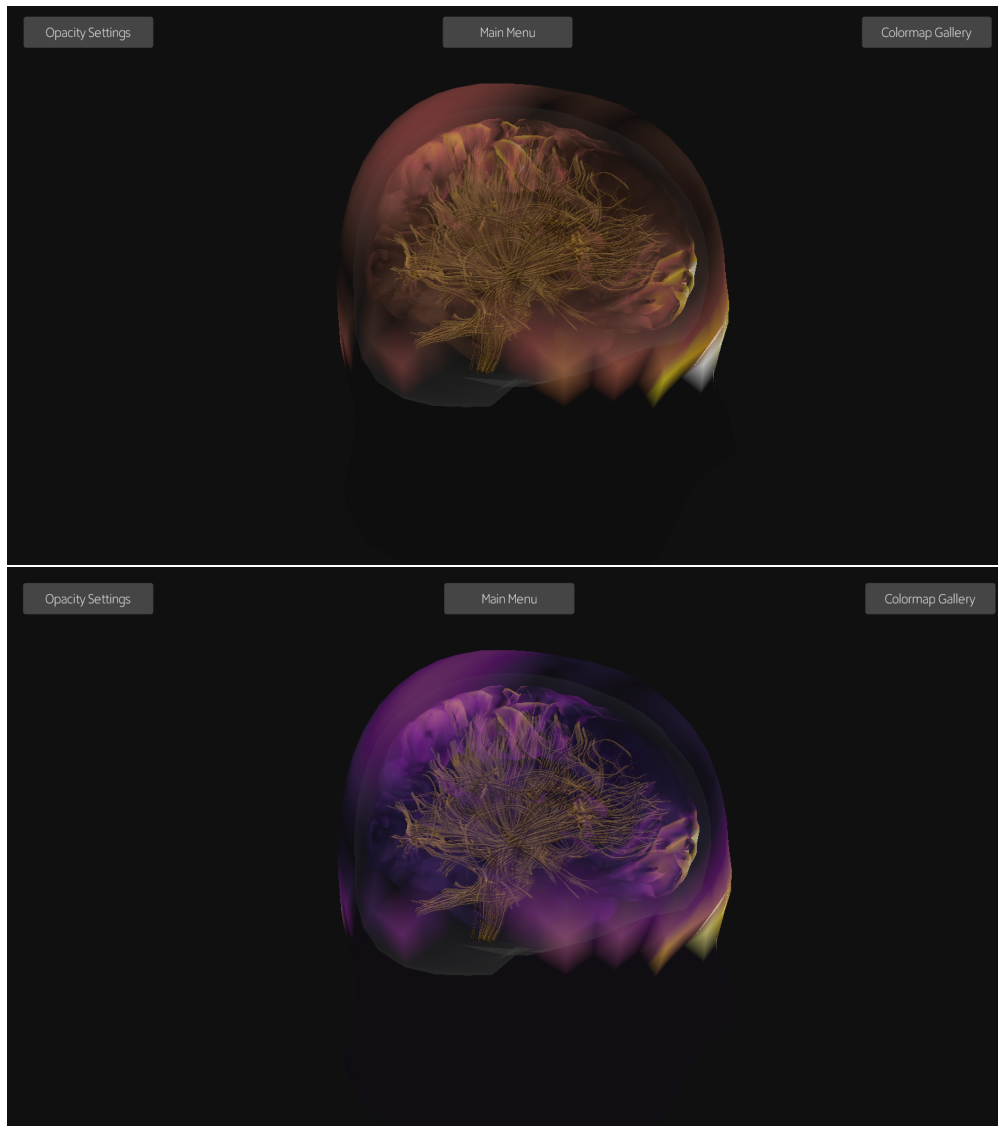


**Figure 3.5:** The electrical activity in Neurosurf, seen with different colormaps.

## Chapter 4

# 3D representation of Brain Models

In this chapter we will show how to represent correctly the corresponding 3D model of an MRI. To do this, we will distinguish two kind of informations given from the same subject.

**T1 Weighted Images:** thought of as the most 'anatomical' of images, T1 weighted sequences result in images that most closely approximate the appearances of tissues macroscopically, although even this is a gross simplification. The dominant signal intensity of different tissues are:

- Fluid (low intensity, black color)
- Muscle (intermediate intensity, grey color)
- Fat (high intensity, white color)
- Brain - gray matter (intermediate intensity, grey color)
- Brain – white matter (hyperintense, white color)

**Diffusion Weighted Images:** Diffusion Weighted Imaging (DWI) assesses the ease with which water molecules move around within a tissue. It represents the combination of actual diffusion values and T2 signal.

To get a complete brain model including anatomy and tractograms we need both these two data. A complete dataset is given from OpenNeuro [13] which offers anatomical images (T1W) and diffusion weighted images (DWI). Indeed, we can divide the work in two phases:

- Head and brain model processing using T1w images through SimNIBS
- Tractogram processing using DWI images through the software MRtrix3, DIPY library

## 4.1 Head and Brain model reconstruction

SimNIBS offers several tools to analyze brain images. In particular, the python code that is able to reconstruct the head model is called `headreco`. It works with T1w images and it gives as a result the 3D model of a head, including skin, skull and brain. An example of how the code works is:

```
headreco.py all CERL_head sub-CON02_ses-preop_T1w.nii.gz
```

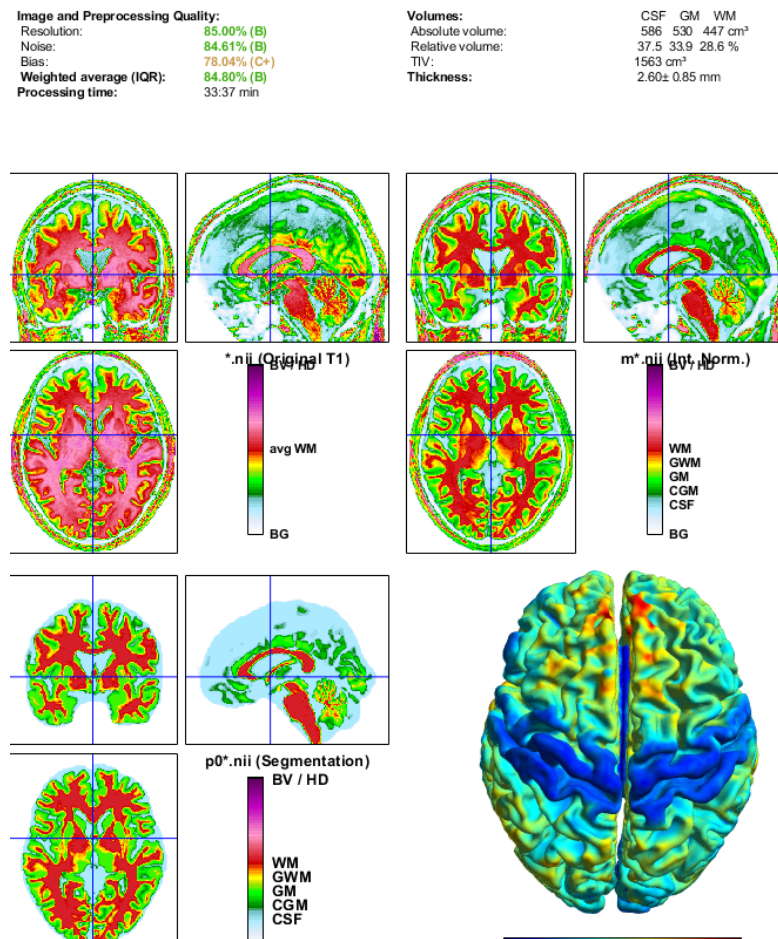
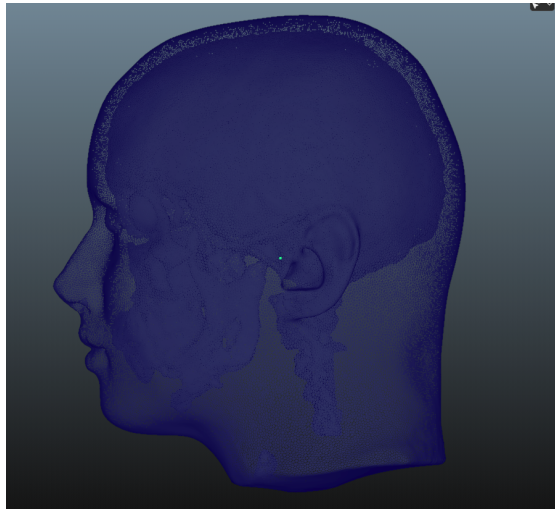


Figure 4.1: Image processing in Matlab.



**Figure 4.2:** 3D model output in Blender 2.9.

where the argument “all” tells headreco to run all the step of the reconstruction including volume meshing, and the argument is the T1w file corresponding to an MRI of a subject. `CERL_head` is the destination folder. `Headreco` processes the images in Matlab (fig. 4.1) and provides the report of the analysis. The output corresponds to a `.msh` file including all the meshes processed by `headreco` and a `.stl` file for every component of the whole mesh.

The best way to visualize the output is the software Gmsh, where it is possible to visualize all the volumes and to export them in different file extension supportable by 3D environment softwares (e.g Unity, Blender).

## 4.2 Tractogram reconstruction

To analyze the DWI data to get a 3D tractogram, the software used was MRtrix3. All the steps did in MRtrix3 to generate the 3D tractogram were inspired form Andy’s Brain Book [14].

The first step consists on converting the files on a file extension which MRtrix3 can understand, using the command `mrconvert inputfile outputfile` it is possible to convert the file extension of the data into `.mif`, the main file extension of the software. With the command `mrview`, it is possible to visualize the MRI images through the viewer (fig. 4.3).

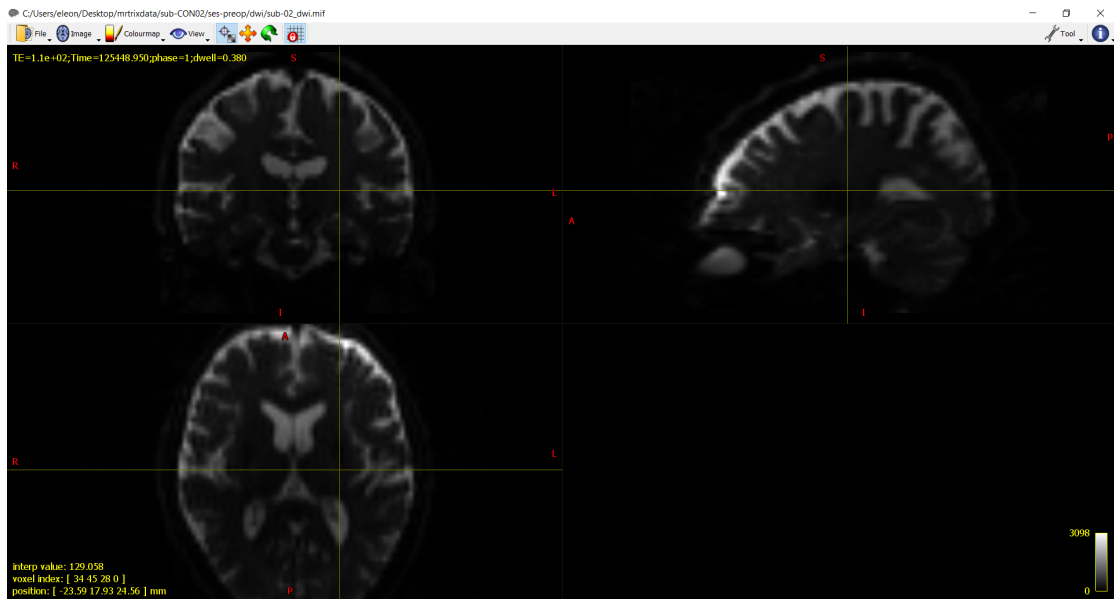


Figure 4.3: MRI image displayed with mrview.

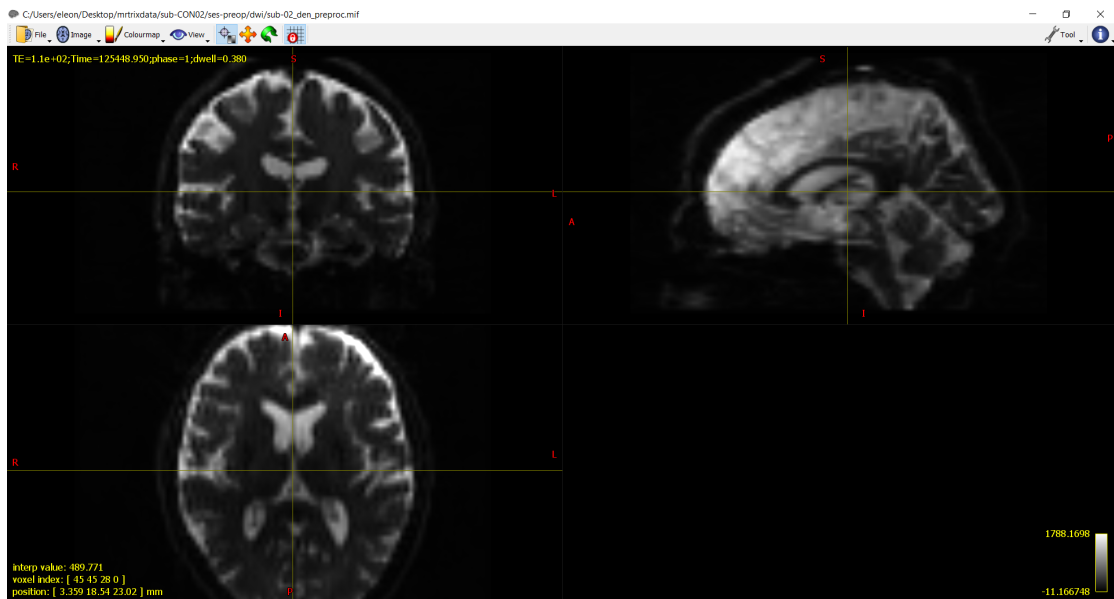


Figure 4.4: Denoised MRI.

## Preprocessing

The further step consists in a phase of preprocessing, which includes denoising and the extraction of the reverse-phase encoded images.

Before talking about preprocessing, we need to introduce two factors: `bval` and `bvec` files. The `bvals` contain a single number per volume that indicates how large of a diffusion gradient was applied to the data; and the `bvecs` contain a triplet of numbers per volume that shows in what directions the gradients were applied. In general, volumes with larger b-values will be more sensitive to diffusion changes, but the images will also be more susceptible to motion and physiological artifacts. The diffusion dataset is composed by two separated imaging files: one that is acquired with primary phase encoding direction and another acquired with reverse phase encoding direction.

The primary phase-encoding direction is used to acquire the majority of the diffusion images at different b-values. The reverse-phase encoded file, on the other hand, is used to unwrap any of the distortions that are present in the primary phase-encoded file. Indeed, what we need is to get an average of the images acquired from the two files, and to do this we have to extract and concatenate the b-values of the two images, that are separated and opposite, and create an average `b=0` images for both phase encoded images.

Once this phase is done we have all the files we need to preprocess them. This can be done through the command `dwipreproc`, which gives as an output all the denoised and preprocessed images (fig. 4.4). To restrict the analysis to the brain voxel, we can use the command `dwibiascorrect` which removes inhomogeneities to get a better mask estimation, and then use `dwi2mask` which restricts the mask to the brain voxels within the brain.

## Basis Function and FOD

In order to determine the orientation of diffusion within each voxel, we will create a basis function from the subject's own data. MRtrix derives the basis function from the diffusion data using the command `dwi2response`, which deconvolves the fiber orientation distribution. In other words it decomposes the diffusion signal into a set of smaller individual fiber orientations. The output shows which voxels were used to generate the basis function for each tissue (fig. 4.5).

The basis function can be used to get the Fiber Orientation Density (FOD), that is an estimate of the amount of the diffusion in each of the three orthogonal directions. To do this we can use the command `dwi2fod` to apply the basis functions to the diffusion data (fig. 4.6).

## Creation of the tissue boundary

The creation of the tissue boundary between the grey matter and the white matter is necessary to avoid the streamlines to terminate in uncorrect points. The anatomical image will be segmented in five different tissue types: grey matter, subcortical grey

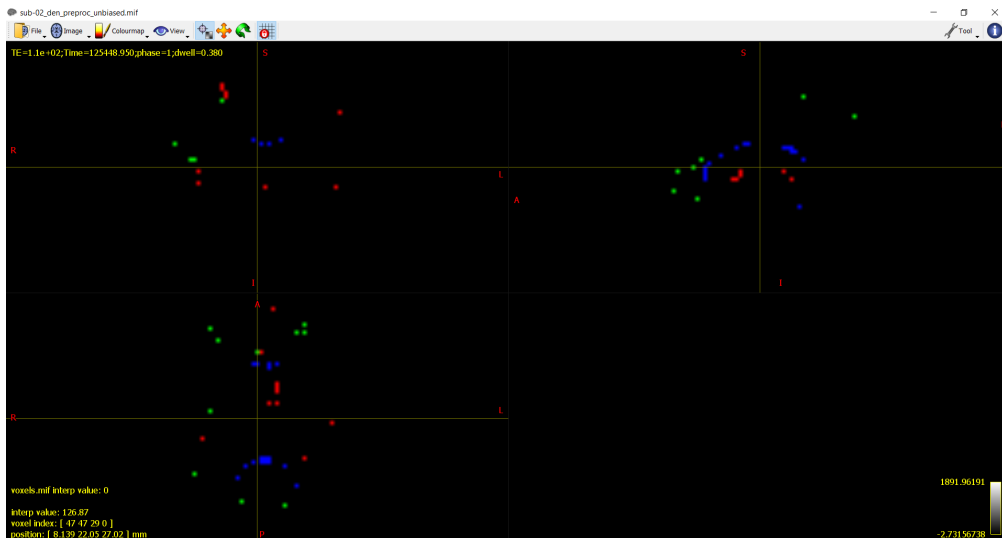


**Figure 4.5:** Red: CSF voxels; Green: Grey Matter voxels; Blue: White Matter voxels.

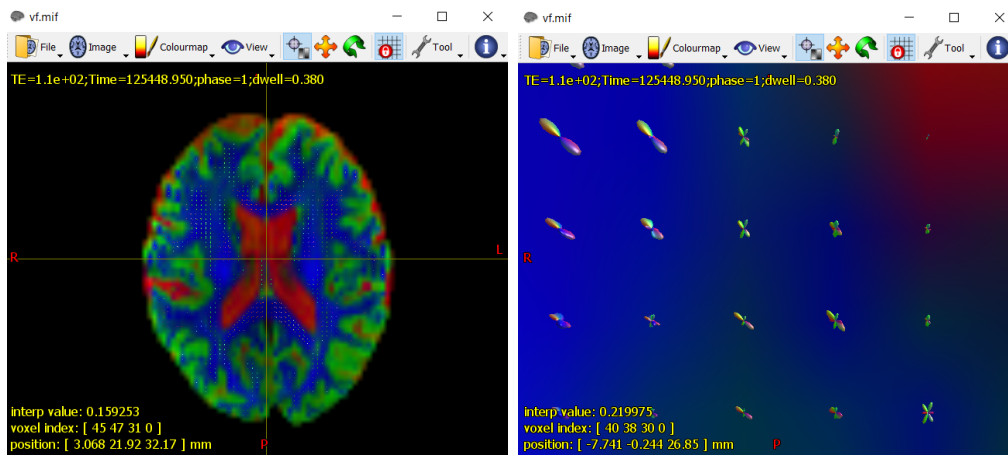


**Figure 4.6:** Fiber Orientation Density (FOD) in the 3D space.

matter, white matter, cerebrospinal fluid and pathological tissue. This will be done using the command `5ttgen`.

After having created the tissue boundary, we can use it as a mask to restrict the area where we will place the seeds from where the streamlines will grow and trace a path. The output of `5ttgen` shows four tissue types in fig. 4.7 (no pathological tissue detected).

The next step is to coregister the anatomical and DWI images to ensure that the boundaries of the tissue types are aligned with the boundaries of the diffusion



**Figure 4.7:** Tissue types generated with `5ttgen`. From the left: grey matter, subcortical grey matter, white matter, cerebrospinal fluid.

weighted images. The commands used will be `dwiextract` and `mrmath` to average the B0 images from the diffusion data. The first one takes the preprocessed diffusion-weighted image as an input and extracts the B0 image, the second one takes the output of `dwiextract` and computes the mean along the 3rd axis which indicates the time dimension. The prefix B0 indicates that a diffusion gradient was not applied during the acquisition of the images, so the b-value is zero.

To use the coregistration command we will use FSL’s `flirt`. This command uses the grey matter segmentation as the reference image, and moves the B0 images to the best fit with the grey matter segmentation. The output will be the transformation matrix that was used to overlay the diffusion image on top of the grey matter segmentation. Once this is done we can coregister the anatomical image to the diffusion image taking the inverse of the transformation matrix with `mrtransform`. The output must be visualized to check the quality of the coregistration. The next

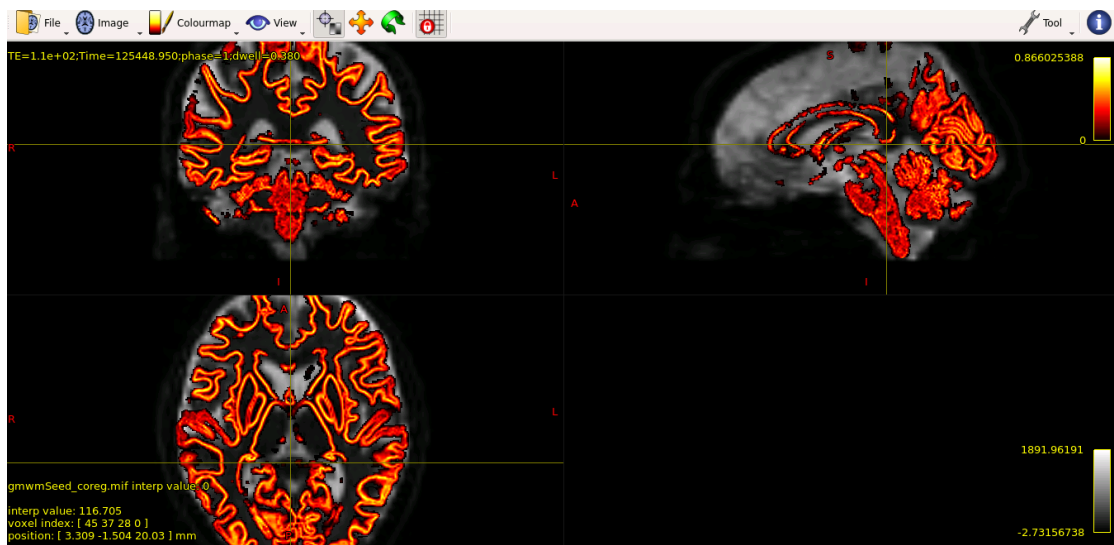


Figure 4.8: Seed boundary.

step is to create the seed boundary separating the grey matter from the white matter with `5tt2gmwmi` which takes as an input the coregistered image and gives as output the seed boundary image (fig. 4.8).

### Generation of the Streamlines

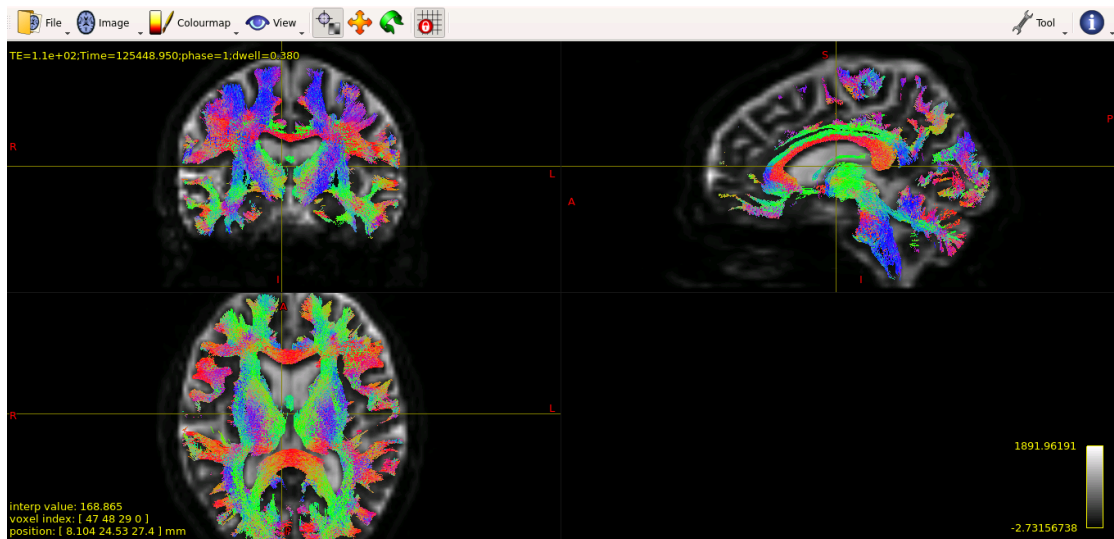


Figure 4.9: Streamlines generated with `tckgen`.

MRtrix3 uses ACT (Anatomically Constrained Tractography). This method

will exclude each streamline which is not biologically plausible e.g. if it terminates in a tissue that is not the gray matter. It is included in `tckgen`, which generates the streamlines. MRtrix uses the probabilistic tractography: multiple streamlines are generated from seed region all along the boundary between grey matter and white matter, their direction will follow the predominant fiber orientation density. In this case we will generate 10 million streamlines with `tckgen`. The complete code is:

```
tckgen -act 5tt_coreg.mif -backtrack -seed_gmwmi gmwmSeed_coreg.mif
-nthreads 8 -maxlength 250 -cutoff 0.06 -select 10000000
wmfod_norm.mif tracks_10M.tck
```

where `-act` specifies that we are using anatomically segmented images, `-backtrack` forces the current streamline to go back and run the same streamline again if it terminates in a wrong area, `-maxlength` sets the maximum track length permitted and `-cutoff` specifies the FOD amplitude for terminating a tract. `-seed_gmwmi` takes as an input the grey matter/white matter boundary generated with `5ttgmwmi`. `-nthreads` is used to specify the number of processing cores you want to use, `-select` indicates how many streamlines to generate. The output is shown in fig. 4.9.

### 3D representation of the Streamlines

To get a 3D model of the streamline, we first need to resample them and then convert them into a 3D readable file extension. To do this, we will use some DIPY libraries and tools. DIPY is an imaging library in python which contains specialized method for computational anatomy including diffusion, perfusion and structural imaging. The first step is to load the tck file we got with the command `tckgen`, then resample it and apply a cluster algorithm, in this case DIPY's QuickBundles.

The source code for this script is presented in appendix A and the output images are shown in fig. 4.10, fig. 4.11 and fig. 4.12.

Now that we have a subsampled set of streamlines, we can convert them in the .ply file extension through MRtrix's `mrconvert` and then import the mesh in Blender, where we can manipulate it.

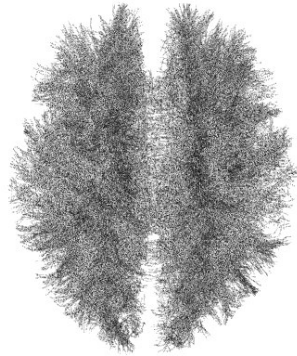


**Figure 4.10:** Initial display of the 3D track.

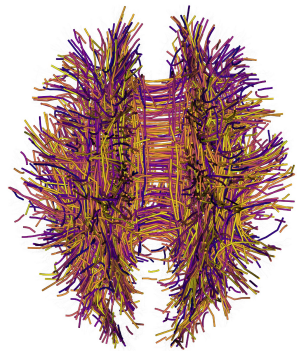


**Figure 4.11:** Track after clustering, with random colors.

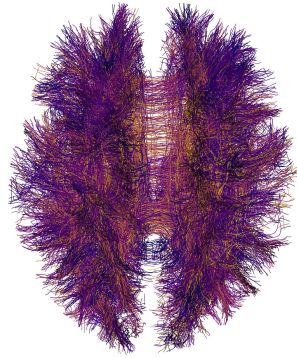


**Figure 4.12:** Different clusters by random colors.



## Chapter 5

# Brain features for brain model selection

As we mentioned in chapter 1, the aim of this work is to give a real-time 3D representation of the brain during a mental task recorded by an EEG, without necessarily having a patient-specific MRI.

The idea was to find a way to give the Neurosuf user the opportunity to see a brain model which is not properly his brain (since an MRI was not performed) but is the brain which best fits his one. The first step is then to dispose of several brain models in order to select the most similar to the user's brain. To do this, we used an open-source dataset given by OpenNeuro composed of 145 subject (79 females, 66 males) aged 17-35 (median 23.46) [13].

This dataset provides all the data we need to reconstruct a 3D model of a human head, for each subject. The typical output of the model reconstruction is shown in fig. 5.1 and is composed by five layers. All the models of the dataset were generated, using the command `headreco` (section 4.1) of the software SimNIBS section 3.2 to create the meshes and an automation algorithm to iterate the reconstruction.

Once we had all the models, the second step was to find the discriminating features to assign a brain model to the user's head. Afterwards several researches in the literature, we found that the discriminating factors for a reliable brain model association are generally:

- Brain volume;
- Head circumference;
- Body Mass Index (BMI).

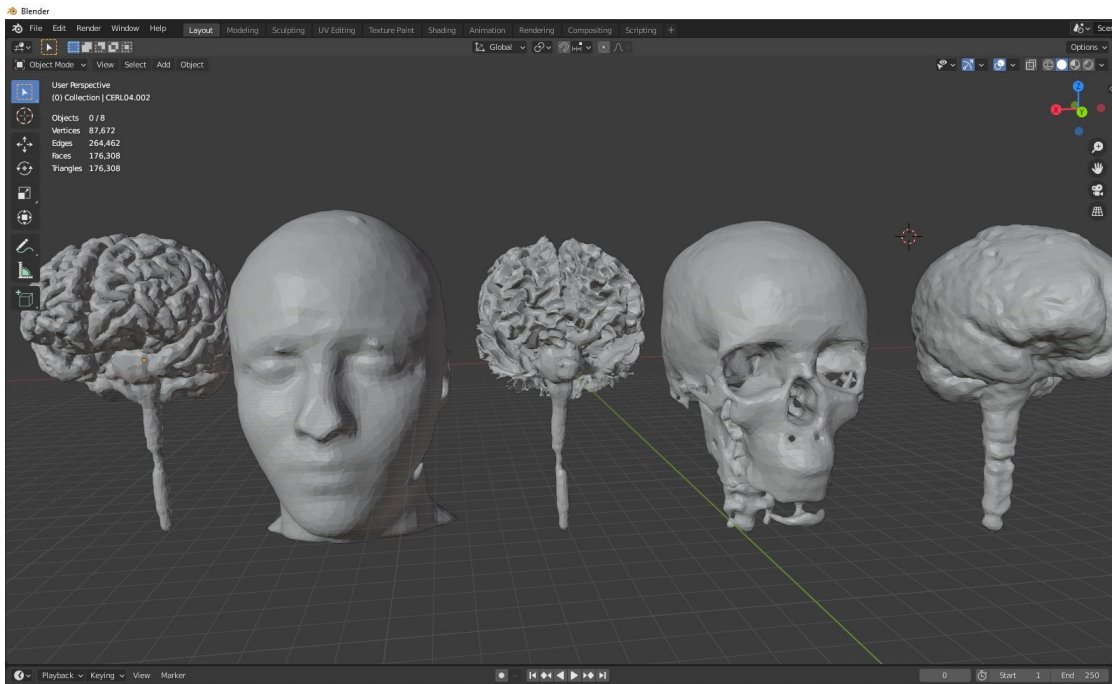


**Figure 5.1:** An overview in Blender of the different layers generated with headreco. From the left: gray matter, scalp, white matter, skull, cerebrospinal fluid.

## 5.1 Brain Volume

As we must assign the brain which most fits the user’s brain, the main thing is to find which characteristics are discriminating to define the structural-functional similarities between a brain and another. Brain volume is assumed to be strictly related to functional activity and behavioral abilities, which are in turn related with neural activity.

Zhao Qing [15] studied the relationship between brain volume and the amplitude of low frequency fluctuation (ALFF), which is said to be related with cognitive performance. Indeed, in specific disease processes (such as epilepsy) these two factors change in a proportional and synchronous way. Qing led an experiment to test the correlation between brain volume and ALFF in two large and independent groups of young adults. For each subject a structural MRI to determine the brain volume and a resting state-fMRI to extract the ALFF measures were performed. From the MRI images three categories of data were extracted:

- grey matter (GM), white matter (WM) and cerebrospinal fluid (CSF) probability/density map in the  $T_1$  native space;
- spatial transformation from the MNI space (which defines the boundaries

around the brain) to the  $T_1$  native space;

- GM, WM and CSF probability/density or volume maps in the MNI space.

Then, a whole-brain ALFF was calculated to compare it with the brain volume. The results obtained comparing the brain volume and the ALFF (fig. 5.2) were consistent and showed a linear correlation between the factors.

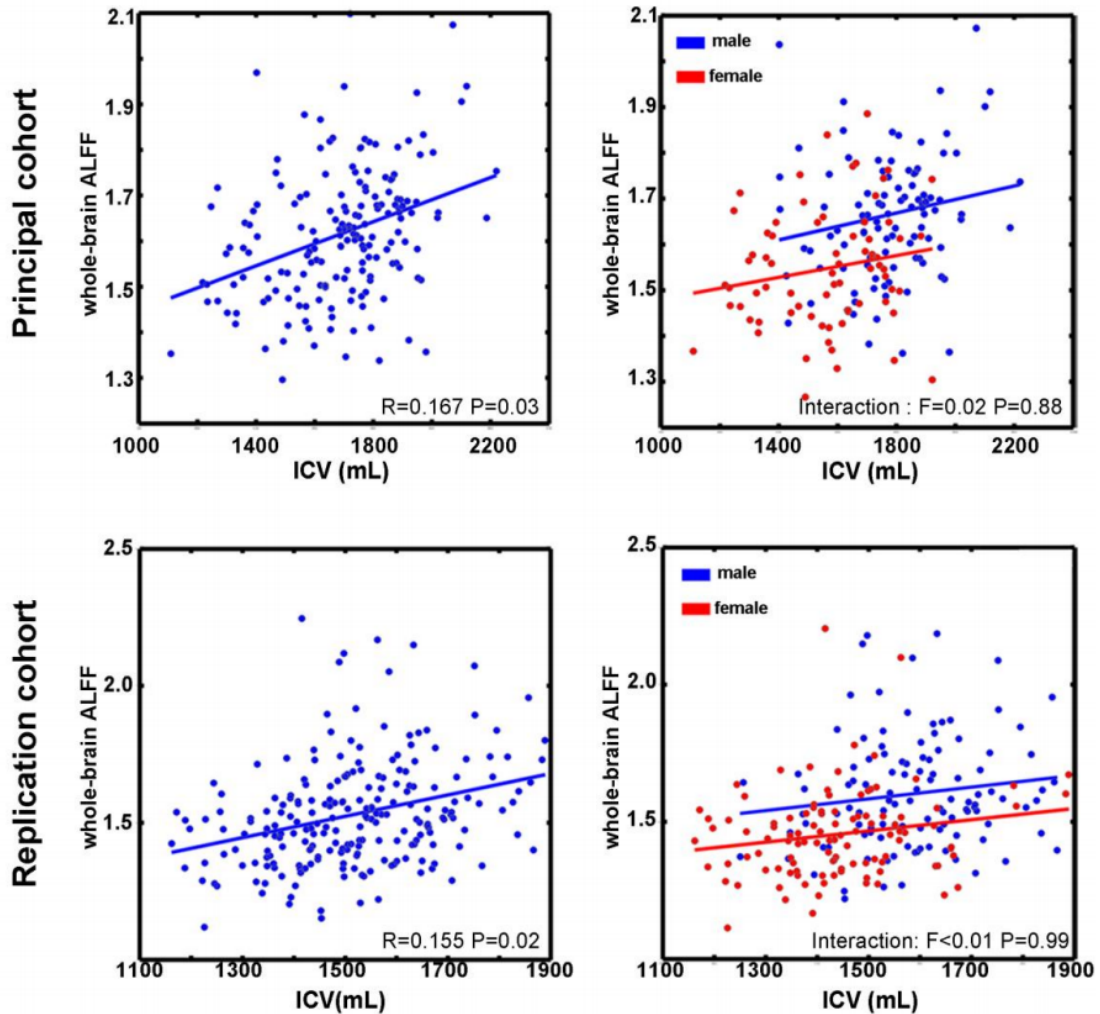


**Figure 5.2:** Correlations between intracranial volume (ICV) and whole-brain ALFF, for the two groups tested. [15]

The brain volume can be then defined as a discriminating factor to associate with functional neuronal activity. In the following sections we will therefore discuss the methods to predict brain volume.

## 5.2 Head circumference

This topic has been investigated by several scientist, and there are different constraints to consider in order to choose the head circumference as a discriminating factor.

The first thing we must regard is the age of the patient. Indeed, the growth of the brain is strictly related to the growth of the head, but only in infancy and early childhood. From the adolescence onward, the brain starts his volume loss and decreases, while the head does not. This does not mean that head circumference and brain volume are not related, but it means that to use properly the head circumference as a discriminating factor to predict the brain volume, we must consider the age of the patient.

To explain better this topic, we could say that we cannot compare the brain of a child to the brain of an adult with a small head, since we have to take into account that the adult's brain started its volume loss from his adolescence, thus its brain will have a smaller volume. Only grouping by age we can use the head circumference as a discriminating factor, especially if we use a dataset with a large range of age.

H.H. Bartolomeusz [16] deepened this topic by taking an experiment which involved 76 subject with a large range of age (from 1,7 to 46). The aim was to quantify the relationship between head circumference and brain volume, and to show how this relationship is affected by age. Axial MR images were performed to all the subjects either.

To calculate the head circumference, the MR  $T_2$ -weighted images were compiled to get a 3D representation of the head, which was re-sliced axially at the level and angle of maximal distance between frontal and occipital lobes. The plane obtained included the occipital protuberance and the most prominent part of the forehead, superior to the eyebrows. Then the comparison between the circumference calculated and the brain volume was performed, taking into account the age, the linear head circumference and the quadratic head circumference. The results obtained are shown in fig. 5.3 and fig. 5.4.

At this point, we can say that brain volume is a reliable discriminating factor, since it is strictly related with neuronal activity as showed in the previous section. We also saw that head circumference computation helps in predicting brain volume if constraints like the age of the subject is considered.

## 5.3 Body Mass Index

The Body Mass Index (BMI) is another factor which could be taken into account to predict the brain volume or the brain weight. In fact, given the strong correlation

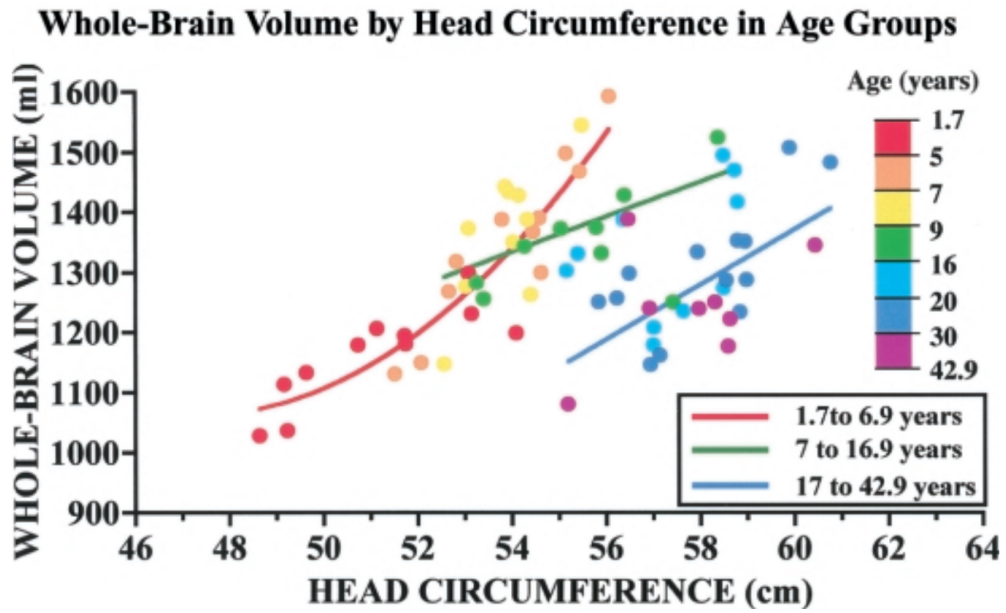


**Figure 5.3:** Relationship between head circumference and brain volume, not grouped by age. [16]

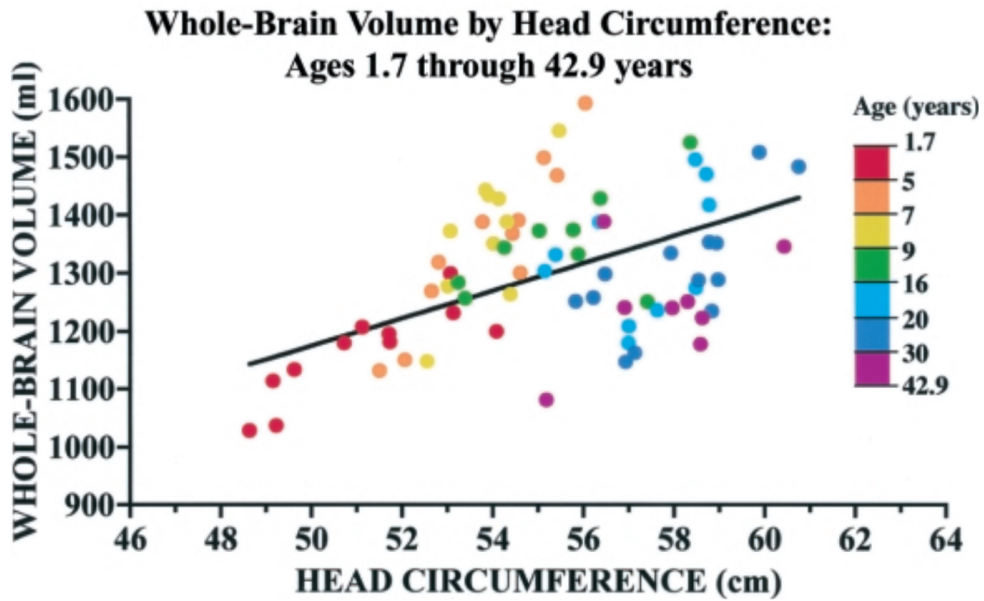


**Figure 5.4:** Relationship between head circumference and brain volume, grouped by age. [16]

between height and weight, these measures could be interchangeable for relating body size and head size. However, this factor is influenced by several other factors including the age which was also a constraint on predicting the brain volume starting from the head circumference.

In particular, if we consider the BMI as a discriminating factor we also should take into account the ethnicity and the gender of the subject. In fact, certain ethnic groups which are typically tall and slender have a different relationship between BMI and brain weight than ethnic groups which are more heavily built [17].

### **Feature selection problems**

This is the theoretical background concerning the association of brain models on the basis of functional characteristics. In reality, these concepts are more easily applicable from a purely medical point of view than from an engineering point of view. The main problem in applying these techniques in a context like that of an interactive application is clearly that of having to guarantee to each user the possibility to have a correct measurement of the circumference of his own head. In fact, the circumference of the head is not a parameter that can be expressed in computational terms in a standard way, as it would be if it were a perfect circumference. There are several irregularities and variable factors that require a precise measurement, which would be effective in an experiment involving a certain number of people, as in the experiments just analyzed. We have also seen that the head circumference is strongly constrained by factors such as the age of the subject in question, which is essential for a correct evaluation of the association of the models.

The aim of this work is to have a dataset of brain models that is as large as possible in order to have as correct an association as possible, which makes grouping by age difficult. Thus, this kind of approach is not the one which suits the best to our project. To predict the best brain fitting we will use then techniques which are most application-oriented, there is to say that we will approach with a computational selection based on algorithms which refer to the Forward Problem (section 2.5) and the Inverse Problem (section 2.6).

## Chapter 6

# Application-Oriented Model Selection

In the previous chapter, we introduced the theoretical methods to define the discriminating features of the brain and to predict the brain volume. In this chapter, we will give an overview of the computational methods we used to do an Application-Oriented association. In particular, we will focus on the topics examined in chapter 2 for the EEG Source Imaging. The equation which describe the potential on the electrodes starting from a distribution of current dipole sources is

$$\mathbf{V} = \mathbf{G}\mathbf{D} + \mathbf{n}. \quad (6.1)$$

where  $\mathbf{V}$  indicates the  $N$ -by- $T$  matrix of the potentials measured at different times at the electrodes positions,  $\mathbf{G}$  indicates the  $N$ -by- $p$  gain matrix,  $\mathbf{D}$  indicates the  $p$ -by- $T$  matrix of the magnitudes of the dipoles at different time instants, and  $\mathbf{n}$  is a noise distribution. Starting from this point, we will do a model association based on the solution of the Forward Problem (FP) and Inverse Problem (IP).

### 6.1 Focal Seizures and single dipole sources

Focal Seizures, or localized seizures are epileptic attacks which affect only one hemishpere of the brain. The brain is subdivided into two hemishperes, and a focal seizure can affect a lobe of the hemisphere where the seizure starts or the whole hemisphere. If we could sample the brain activity while a seizure is in progress we could observe a very focal activity that we could model, in first approximation, with an active dipole in the interested region while all the other dipoles in the model are inactive. In terms of coefficients, in the previous equation this is translated in

a column of  $D$  with all zeros except the coefficient of the active dipole that will have a magnitude relative to the one of the noise component.

In the Forward Problem, the electric potential  $V$  is calculated starting from an hypothetical single dipole with a specific behavior.  $V$  is represented as a matrix of the potentials measured at different times. We will focus on focal seizures, thus calculating the potential starting from a single epileptic dipole source. We will call  $v$  the vector which indicates the potential measured at one generic time instant. To get  $v$ , the gain matrix  $G$  or lead-field matrix is multiplied by the column vector  $d$  of the single epileptic dipole. Then, considering the potential detected at one generic time instant, starting from a single epileptic dipole source we have:

$$v = Gd + n. \tag{6.2}$$

## 6.2 Electrical Potential determination with a reference dipole

To introduce our technique of source localization using a reference model, we will first approach with the Forward Problem.

As we mentioned in chapter 4, through MRI processing techniques it is possible to get a complete and reliable 3D model which represents the various head layers of the subject for which the MRI was performed. Then, we suppose that this subject is affected by Focal Epilepsy (seizures). This subject will be our reference.

In the previous section, we said that the behavior of an electric dipole which generates a seizure can be predicted. To calculate the lead-field matrix  $G$ , which is necessary to obtain the potential  $v$  at a determined point in the surface of the head, we need:

- the head volume, generated with MRI processing;
- a given electrode setup.

The electrode setup can be reliably estimated through a specific software e.g. Simnibs, which refers to the volume generated by the MRI processing (fig. 6.1).

The EEG position are calculated by visually determining the positions of the nasion (Nz), left preauricular point (LPA), right preauricular point (RPA) and inion (Iz). These are the 4 fiducial points based on the UI 10/10 definition. Thus, running the command

```
eeg_positions -m CERL.msh -o CERL_10_10_10 -Nz 7.24 100.12 1.64
-LPA -72.03 10.38 -5.00 -Iz -6.20 -79.49 4.26 -RPA 73.83 2.36 -9.85
```

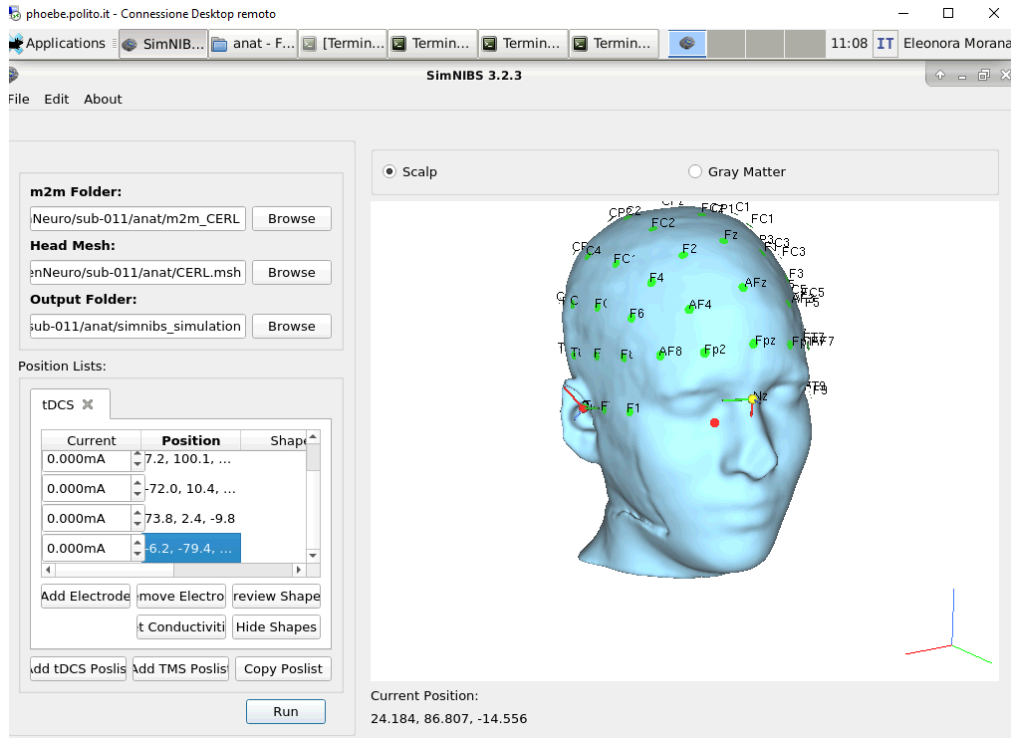


**Figure 6.1:** Calculation of the 10/10 EEG positions based on 4 fiducial points based on the UI 10/10 definition.

The EEG positions are generated and the lead-field matrix can be calculated. The reason why we need this electrode setup is that the lead-field  $G$  is the matrix which takes into account all the position vectors  $r$  referring to the real positions of each electrode in the head surface, referring to a determined dipole with a position vector  $r_{dip}$  and orientation  $e$ . Without the electrode setup referring to the head model, we can't determine the position vector  $r$ . At this point, we have the vector  $d$  of the epileptic dipole, which will be placed in the layer of the cerebral cortex, the lead-field matrix  $G$  and we can calculate the potential  $v$  for the subject affected by focal seizures.

## 6.3 Model association

Once we have calculated the electric potential  $v$  by solving the Forward Problem, our aim is to find the model which is the most similar to our reference, considering all the model present in our dataset. To do this, we will approach with the Inverse Problem. We suppose to have all the lead-field matrix  $G$  referring to each brain model, and the same dipole  $d$  we used to solve the FP. Now, we will call  $v_{ref}$ ,  $G_{ref}$

and  $d_{ref}$  respectively the electrical potential vector of the reference, the gain matrix of the reference and the electrical source dipole of the reference. The dipole has a position of  $(x_{ref}, y_{ref}, z_{ref}) = r_{ref}$ . We now suppose to have 3 models referring to 3 different subject in the dataset. The four equations corresponding to the current flow model of the subjects will be:

$$\mathbf{v}_{ref} = \mathbf{G}_{ref}\mathbf{d}_{ref} + \mathbf{n}; \quad (6.3)$$

$$\mathbf{v}_1 = \mathbf{G}_1\mathbf{d}_1 + \mathbf{n}; \quad (6.4)$$

$$\mathbf{v}_2 = \mathbf{G}_2\mathbf{d}_2 + \mathbf{n}; \quad (6.5)$$

$$\mathbf{v}_3 = \mathbf{G}_3\mathbf{d}_3 + \mathbf{n}. \quad (6.6)$$

Then, we assign to each model the electrical potential  $v_{ref}$  of the reference, since we want to compute where would be the dipole source if the electrical potential detected on the scalp was the same of the reference. In other words, we are supposing that all the four subjects are affected by seizures and that the potential  $v$  detected is generated by the same epileptic dipole source. So we have that

$$\mathbf{v}_1 = \mathbf{v}_2 = \mathbf{v}_3 = \mathbf{v}_{ref}. \quad (6.7)$$

In order to find the positions  $(x, y, z)$  of the dipole sources of each subject, we have to approach with the Inverse Solution and compute

$$\mathbf{d}_1 = \mathbf{G}_1^{-1}\mathbf{v}_{ref}; \quad (6.8)$$

$$\mathbf{d}_2 = \mathbf{G}_2^{-1}\mathbf{v}_{ref}; \quad (6.9)$$

$$\mathbf{d}_3 = \mathbf{G}_3^{-1}\mathbf{v}_{ref}. \quad (6.10)$$

With  $d_1$ ,  $d_2$  and  $d_3$  respectively in  $(x_1, y_1, z_1) = r_1$ ,  $(x_2, y_2, z_2) = r_2$  and  $(x_3, y_3, z_3) = r_3$ . By solving these equations, we find 3 different value of each dipole. At this point we calculate

$$\mathbf{err}_1 = \mathbf{r}_{ref} - \mathbf{r}_1; \quad (6.11)$$

$$\mathbf{err}_2 = \mathbf{r}_{ref} - \mathbf{r}_2; \quad (6.12)$$

$$\mathbf{err}_3 = \mathbf{r}_{ref} - \mathbf{r}_3; \quad (6.13)$$

Where  $err_1$ ,  $err_2$  and  $err_3$  are the distance between the reference position vector of the dipole and the position of respectively  $r_1$ ,  $r_2$  and  $r_3$ .

At this point we can say that the minimum error distance will correspond to the model which has the most similar brain structure, since its dipole source is localized as the nearest to the original reference. Thus, its corresponding brain model can be assigned to our reference.

## 6.4 Computational substitution of brain models

In the previous section we defined a model to compute an association based on source localization. In this section we will discuss the parameters to take into account in order to do a physical substitution in a 3D environment.

Each mesh in the 3D space is localized with a center in  $(x, y, z)$  which can correspond to the center of mass of the volume or to the center of the object, there is to say the medium point of the mesh. The mesh has also a scale property which indicates its size in the 3D space. Thus, to give a correct description of a mesh in the 3D space we must consider:

- its center;
- its bounding box.

Where the bounding box (fig. 6.2) is the sphere where all the vertices of the mesh are contained and where the distance between the center of the mesh and the farthest vertex of the mesh corresponds to the ray of the sphere.

As we mentioned in the previous section, the basic idea for the model association is to leave the external layer (the scalp) fixed. This is because the scalps generated with MRI image processing are not - in most cases - defined meshes. The image processing of MRI is detailed for what concerns the internal layers of the head (skull, CSF, grey matter and white matter) but it lacks of precision in the scalp models.

This happens because the scalps are not as important as the internal layers for a structural/functional analysis and because in the MRI present in the open-source datasets the visibility of the scalp is sort of "cut", due to privacy reasons. Thus, we chose a fixed external layer which corresponds to the most accurate we found in the dataset. Leaving fixed the external layer means that all the models we put into that layer should have its center and a precise scaling factor which exactly adapts with the layer of the scalp selected.

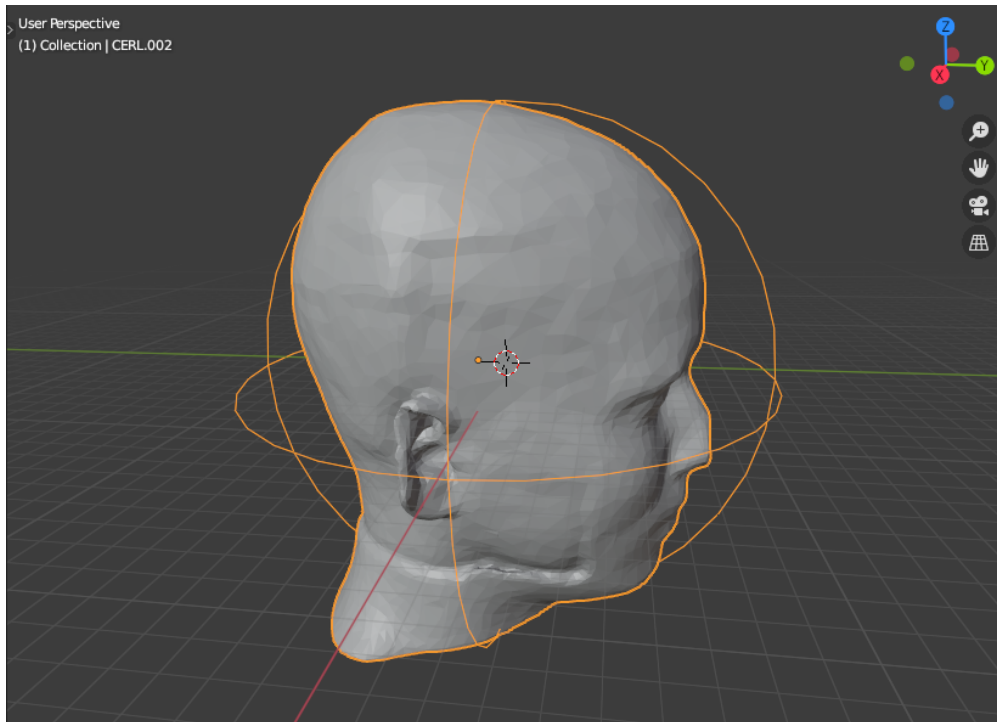


**Figure 6.2:** Example of a 3D model with its bounding box in the 3D space.

## 6.5 Sphere fitting algorithms

In order to center and scale the brain models inside the fixed scalp, an algorithm which re-centers and re-scales all the spheres in a sphere with ray  $r = 1$  in the center of the 3D space  $(0,0,0)$ . The first step is to convert the file extension of each mesh, which is a volumetric mesh `.msh`, into its `.stl` (Standard Triangulation Language) version:

The script takes the `.msh` file as input and gives the `.stl` format as output. Then, the `.stl` output is given as input to the script which re-centers and re-scales the mesh. This script is presented in appendix B.

The codes are written in python and use mathematical libraries such as NumPy and mesh-manipulating libraries such as mesh.io. In this way, all the 3D models of the dataset have the same center in  $(0,0,0)$  and the same bounding box with unitary ray. Thus, all the internal layers can be put into the reference scalp. This model selection that has been presented includes the presence of the MRI of the subject reference.

As we told introducing this project, our objective is to define an algorithm which does not require a patient specific MRI. Indeed, this technique we presented characterizes the first step in the definition of a standardized algorithm of brain

selection, which requires a large model library and some machine-learning training. However, in the following chapters we will discuss the results we got so far and our objective for the future.



# Chapter 7

## Results

The subjects used for testing our algorithms were taken from the dataset described in chapter 4.

### 7.1 Selection of the scalp

As mentioned in the previous chapter, the first thing is to select a scalp which remain fixed while the internal layers change according to the discriminating features of the brain models. After an overview of all the scalp models, we selected the *subject*<sub>011</sub> which appears the most accurate among 145 subjects.

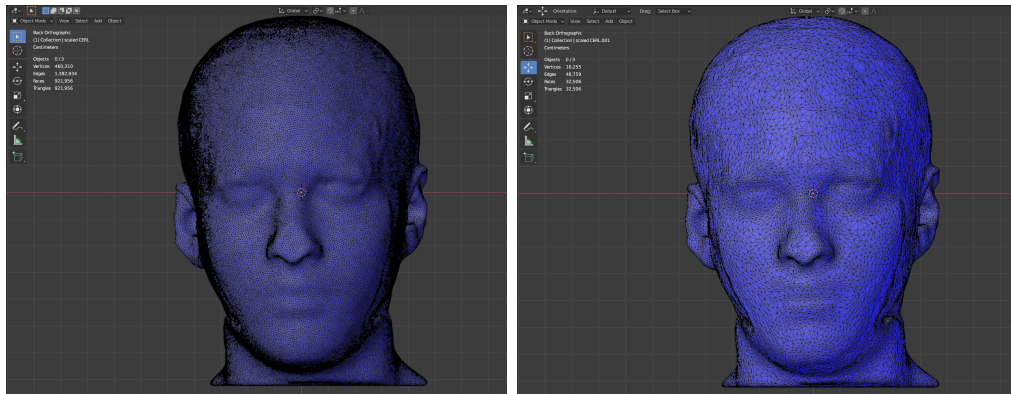


**Figure 7.1:** On the left: subject 11. On the right: Scalp of subject 11, subsampled with ratio 0.2 (Blender 2.9).

The original mesh is very refined (its vertex-count overcomes 400.000 vertices), and using a mesh with this complexity to get the lead-field matrix would result time-consuming. To make the mesh compatible with the electromagnetic solver to generate the lead-field matrix, we used the Blender modifier "Decimate". It allows

to subsample the mesh reducing its vertices given a ratio, which in this case is 0.2 in a range from 0 to 1. In (fig. 7.1), the mesh before and after subsampling is shown.

In our algorithm, this is the layer which remain fixed. It has no internal layers since its task is to be a "container" for all the other subjects' internal layers. Therefore, the sphere-fitting scripts we discussed in the previous chapter were applied to this layer. Thus, it is centered in (0,0,0) and its bounding box has unitary ray.

In the following section, we will give an example of a brain model substitution.

## 7.2 Internal layers substitution

Once we selected and subsampled the scalp, the next step is to try the real sphere-fitting by putting another group of internal layers in the scalp selected.

We will put the internal layers of *subject*<sub>012</sub> inside the scalp reference to verify the success of the sphere-fit algorithm, after having subsampled the mesh.

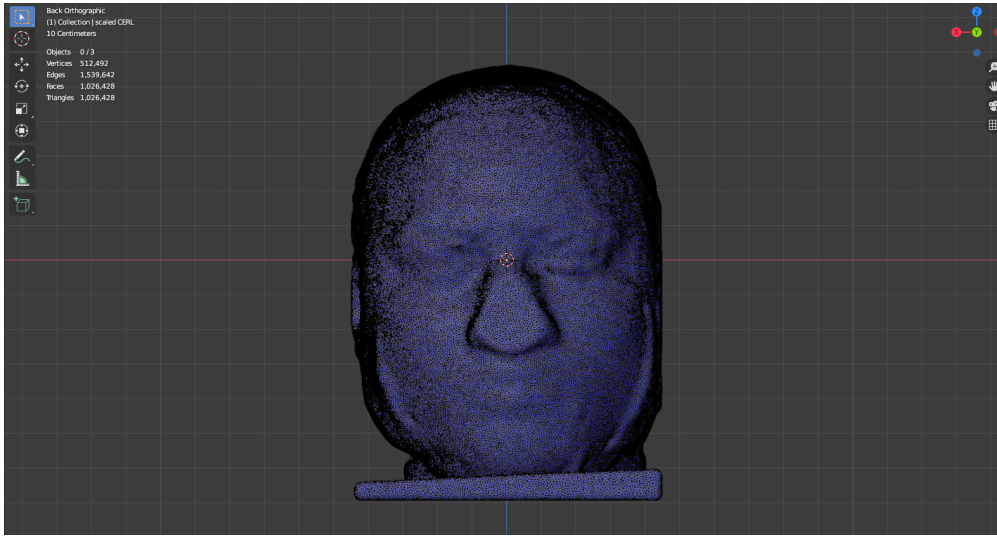


**Figure 7.2:** Scalp of subject012.

As we mentioned in the previous chapters, the reason why we choose to keep a fixed scalp is that some errors can occur during the generation of scalps during the MRI image processing. For example, as we can see in (fig. 7.5), an accidental plane in the bottom of the head was generated for the *subject*<sub>012</sub>.

The sphere-fitting script is applied to *subject*<sub>012</sub> so that its center is (0,0,0) and its bounding box has ray 1. Its internal layers (skull, cerebrospinal fluid, grey

matter and white matter) are put into the reference scalp. The internal layers are shown in fig. 7.3

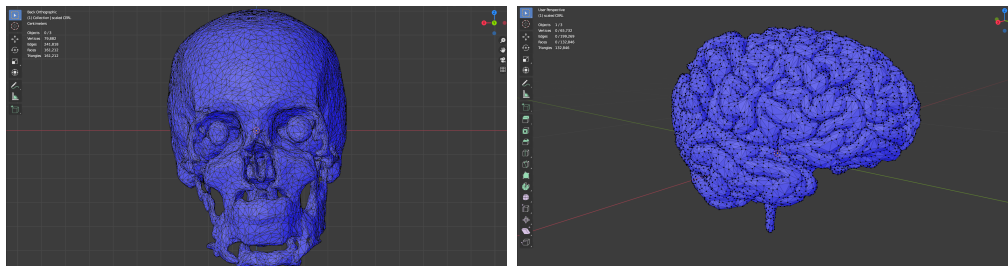


**Figure 7.3:** From the left: Skull of subject012 and Brain of subject012, subsampled with ratio 0.2.

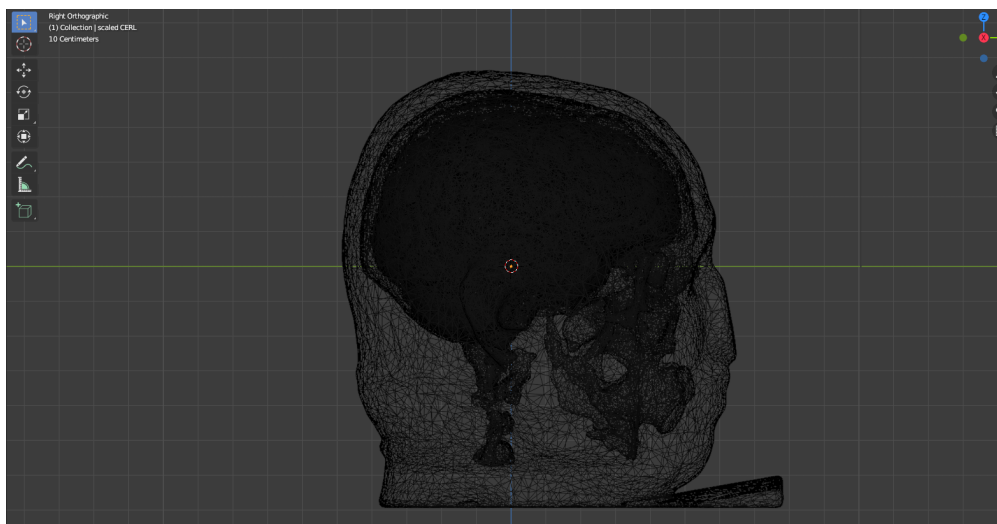


**Figure 7.4:** Scalp of subject012 with its internal layers.

As we can see in (cref) and (cref), the fitting works. The image show also that the pairing is not comfortable, since the shape of the head is completely different from the shape of the internal layers. This is not a problem for us since the task of the reference scalp is just to be an "aesthetic container" and does not have any influence on the source localization. This also confirms that the internal layers of a scalp are strictly related with head circumference and Body Mass Index, that are in fact visually different in *subject*<sub>011</sub> and *subject*<sub>012</sub>.

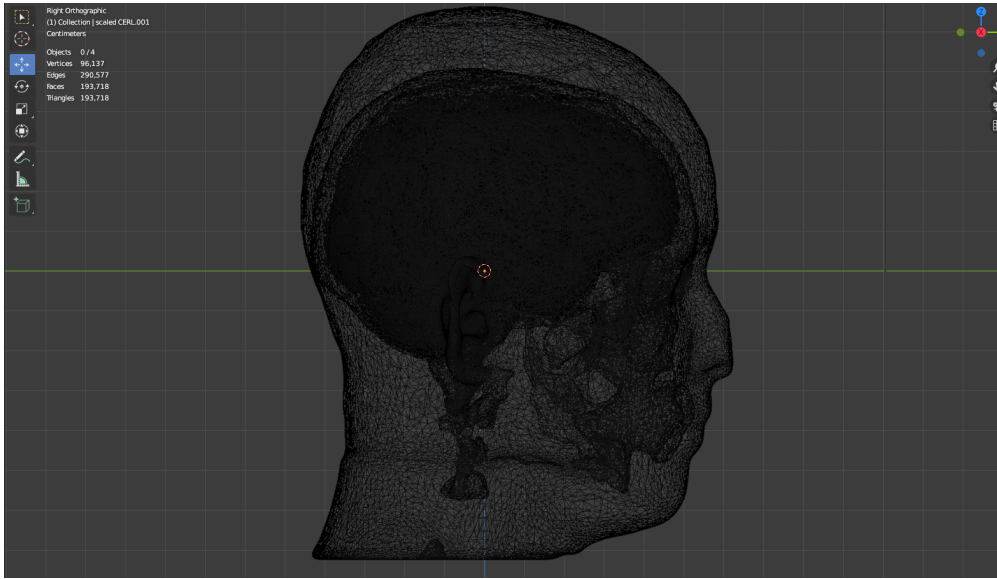


**Figure 7.5:** Reference Scalp with the internal layers of subject012.

### 7.3 Tests of brain model association

Once we assumed that we can work with sphere-fitting, the further step is to try an association of two brain models based on the techniques discussed in chapter 6.

Two subjects were used to test the association. The 3D models were subsampled with ratio 0.05 in order to get a complete 3D model with a maximum amount of 10.000 vertices. The first step consists on calculating the potential at the electrodes with hypothetical dipoles considering:

- original EEG positions;
- EEG positions associated to the vertices of the mesh after the subsampling;
- position of the dipoles;
- moment of the dipoles;
- conductivity of the layers.

The original EEG positions correspond to the electrode setup we discussed in the previous chapter. The reason why we need the EEG positions after the subsampling lies in the fact that the vertices change their position in the 3D space after the subsampling. This means that if we have an electrode associated to a vertex  $v$ ,  $v$  could have been deleted after the subsampling or could have changed its position.

The solution to this problem is to find the nearest vertex to  $v$ , and to associate the electrode to that vertex. To do this, we used a python script which is presented in appendix C. The position of the dipoles corresponds to the vertices of the mesh where we can place the epileptic dipole source, there is to say the position of the vertices of the white matter. To get these position, a brief python script is presented in appendix C.

The conductivity of the layers defines the way a tissue in the human head is more or less resistant to the electrical flow and is expressed in Siemens/meter. It is assumed that the conductivity is 0.41 S/m for the scalp, 0.02 S/m for the whole skull and 0.47 S/m for the grey matter. These are the three layers we will use to test the brain model association.

In our test, we chose to use 3 dipoles generating a seizure as the electrical source. This is because an epileptic dipole source corresponds to an hyperintense neural activity, thus it is easier to record the activity more reliably. Therefore, as we said in the previous chapters, we know the behavior of this kind of dipoles.

The dipoles were placed in the cerebral cortex of the subjects. The Forward Problem is then solved, and for each subject we obtained a matrix that is not properly the gain-matrix  $G$ . Indeed, the gain-matrix can be evaluated considering all the dipole sources which generate a current distribution reaching each electrode on the scalp. In this case, we have only 3 dipoles for each electrode.

The column vectors corresponding to the potential detected for each dipole were plotted and are shown in fig. 7.6, fig. 7.8 and fig. 7.10 for the first subject, and in fig. 7.7, fig. 7.9 and fig. 7.11 for the second subject.

The plots show that, for these dipoles, the potential generated is different even if the dipoles used are the same in both the subjects. This happens because we should consider one dipole for every vertex got from the white matter, then about three thousand dipoles. By doing this, the current distribution detected would be similar for each dipole, the gain-matrix  $G$  would be completed and the Inverse Problem could be solved.

However, to find the Inverse Solution a further work on the meshes is required. The association can be completed by using all the dipoles got from the white matter and it requires an enormous precision on the definition and the manipulation of the meshes that will be included in our future work.

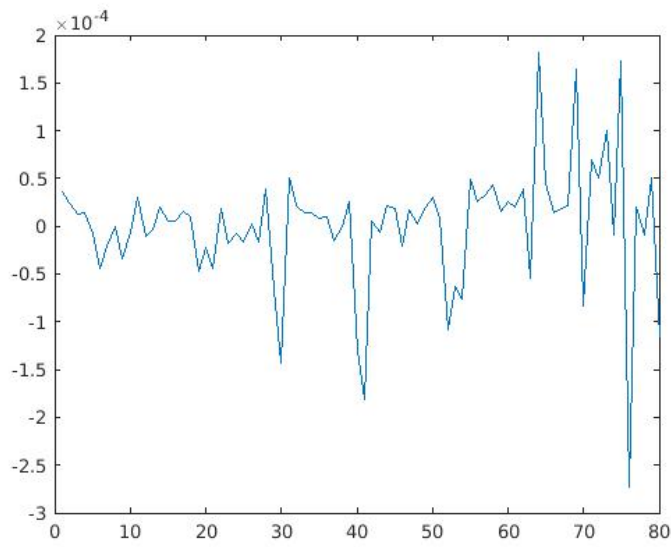


**Figure 7.6:** Plot of the potential detected from the first dipole source (first subject).

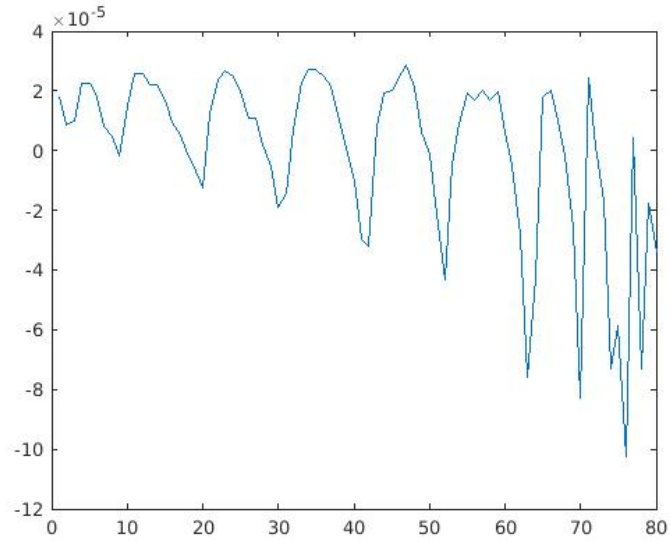


**Figure 7.7:** Plot of the potential detected from the first dipole source (second subject).

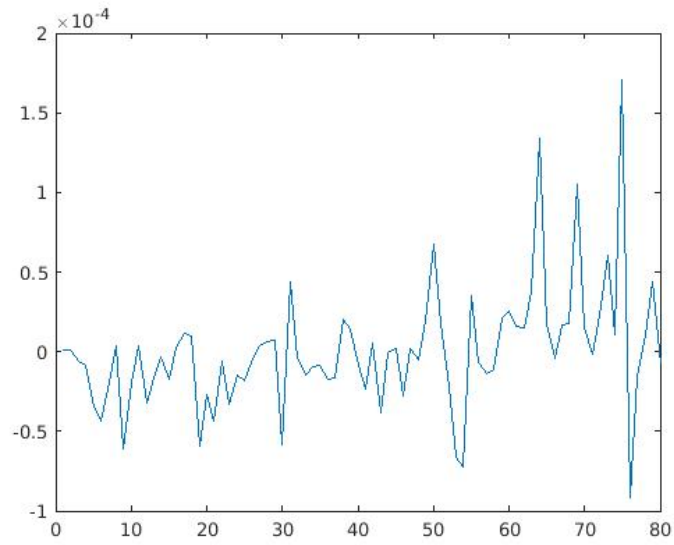


**Figure 7.8:** Plot of the potential detected from the second dipole source (first subject).

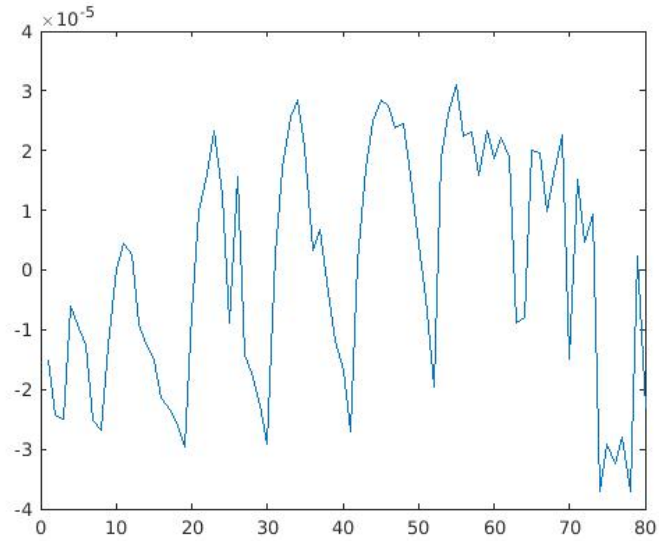


**Figure 7.9:** Plot of the potential detected from the second dipole source (second subject).

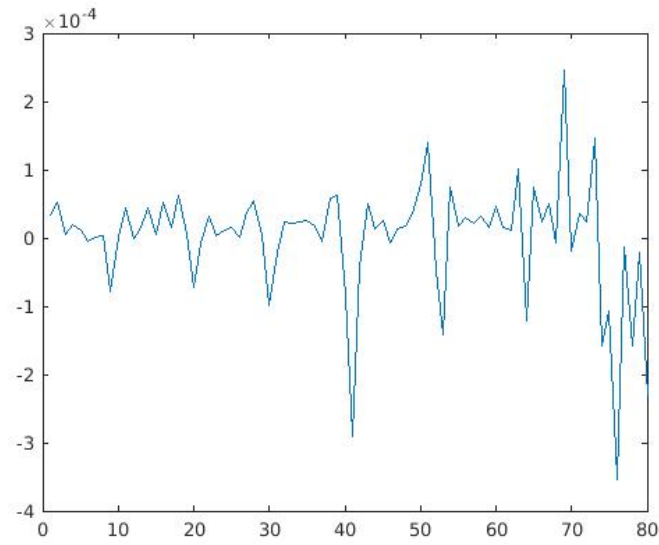


**Figure 7.10:** Plot of the potential detected from the third dipole source (first subject).

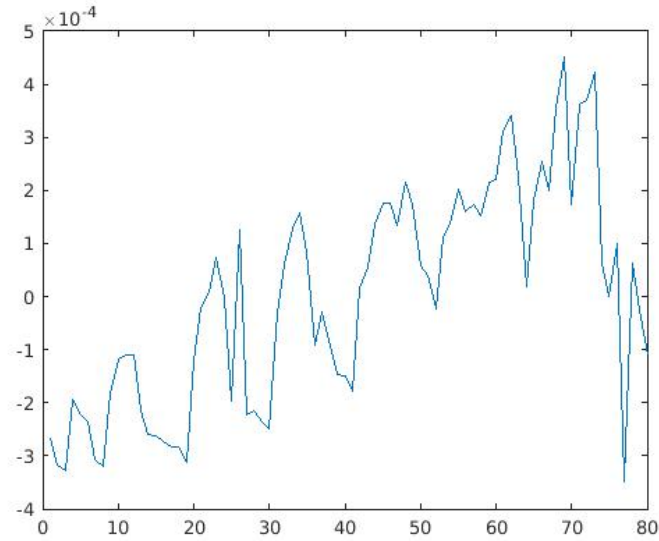


**Figure 7.11:** Plot of the potential detected from the third dipole source (second subject).

## Chapter 8

# Conclusions and future work

From the beginning of this project, the aim was to simplify the techniques of structural and functional analysis of the neural activity. We examined the techniques of EEG Source Imaging to solve the Forward Problem and the Inverse Problem and we combined the source localization with MRI image processing to give a complete experience of VR visualization in real-time.

However, the work done so far requires a further improvement since it is only the starting point to be defined a standardized model of functional and structural reconstruction of brain activity.

We studied the constraints and the limits of brain models association, including the theoretical constraints deepened in chapter 5 and the physical constraints as the ones we examined in the mesh-fitting and brain model association. In chapter 6 we tried to demonstrate how to match the structure of two brain models by solving the Forward Problem and the Inverse Problem, thanks to the theoretical basis which characterize the properties of dipole sources in Focal Epilepsy. However, in this case a patient-specific MRI was included and a deeper work on the brain mapping is required to solve the Inverse Problem.

The further work will be characterized by an accurate definition of the brain mapping based on the improvement of mesh processing and by a phase of Machine-Learning, where the training will be based on the analysis of the known cases we built with our model library. The system will be trained to extract and recognize the localization errors in order to use them as a metric to be minimized. The error minimization, as explained in chapter 6, is the key step which enables the association of brain models based on source localization. The result would be the reconstruction of the brain's electrophysiologic activity without having access to patient-specific MRI.

The development of an automated system based on EEG Source Imaging would be useful in furthering studies regarding mental diseases such as Epilepsy and ADHD. EEG-based analyses, as pointed out many times, are not efficient in their spatial resolution, making a structural-functional study of this kind of diseases difficult. The localization of the sources obtained by EEG Source Imaging would instead allow to recover this spatial resolution, thus enabling non-invasive intracranial explorations with visual neurofeedbacks.

# Appendix A

## Subsampling and Clustering

```
import os
import numpy as np

from dipy.io.stateful_tractogram import Space, StatefulTractogram
from dipy.io.streamline import load_tractogram, save_tractogram
from dipy.io.utils import (create_nifti_header, get_reference_info,
is_header_compatible)
from dipy.tracking.streamline import select_random_set_of_streamlines, Streamlines
from dipy.tracking.utils import density_map
from dipy.data.fetcher import (fetch_file_formats, get_file_formats)
from dipy.viz import window, actor
from dipy.segment.clustering import QuickBundles

track = load_tractogram("smallerTrack_200k.tck", "reference_anatomy.nii.gz")
#loading the tractogram

affine, dimensions, voxel_sizes, voxel_order =
get_reference_info("reference_anatomy.nii.gz")

#getting the informations from the reference anatomy

track=to_voxmm()

#moving the streamlines to the voxel space

track.tovox()
track.tocorner()

#accessing volume informations in a grid
```

```
track_vox=select_random_set_of_streamlines(track.streamlines,10000)

#subsampling the streamlines in 10k streamlines

affine, dimensions, voxel_sizes, voxel_order = track.space_attributes
track_density = density_map(track_streamlines_vox, np.eye(4), dimensions)
track = StatefulTractogram(cc_streamlines_vox, reference_anatomy, Space.VOX)
save_tractogram(track, "track_1000.tck")

#apply the clustering algorithm

streamlines=track.streamlines
qb=QuickBundles(threshold=10.)

#performing QuickBundles using MDF metric and a 10mm distance threshold
#automatic downsampling to 12 points

clusters=qb.cluster(streamlines)

interactive=True
scene=window.Scene()
scene.SetBackground(1,1,1)
scene.add(actor.streamtube(streamlines, window.colors.white))
window.record(scene, out_path='track_initial.png', size=(4096,2160))

#initial track dataset

colormap = actor.create_colormap(np.arange(len(clusters)))
scene.clear()
scene.SetBackground(1, 1, 1)
scene.add(actor.streamtube(streamlines, window.colors.white, opacity=0.05))
scene.add(actor.streamtube(clusters.centroids, colormap, linewidth=0.4))
window.record(scene, out_path='track_centroids.png', size=(4000, 4000))
if interactive:
    window.show(scene)

#centroids of the track after clustering with random colors

colormap_full = np.ones((len(streamlines), 3))
for cluster, color in zip(clusters, colormap):
    colormap_full[cluster.indices] = color
scene.clear()
scene.SetBackground(1, 1, 1)
scene.add(actor.streamtube(streamlines, colormap_full))
window.record(scene, out_path='track_clusters.png', size=(4000, 4000))
```

```
if interactive:  
    window.show(scene)  
  
#showing the different clusters
```



# Appendix B

## Sphere-Fitting

### B.1 Conversion from .MSH to .STL

```
import sys
import os

for filepath in sys.argv[1:]:
    new_filepath_split = filepath.split('/')
    new_filepath_split[-1] = new_filepath_split[-1].split('.')[0] + '.stl'
    new_filepath = '/'.join(new_filepath_split)
    s = 'meshio-convert {0} {1}'.format(filepath, new_filepath)
    os.system(s)
```

### B.2 Centering and Scaling

```
import sys
import numpy as np
import meshio

for mesh_filename in sys.argv[1:]:

    m = meshio.read(mesh_filename)

    p_max = np.max(m.points, axis=0)
    p_min = np.min(m.points, axis=0)

    scale_factor = 1 / np.linalg.norm((p_max - p_min) / 2)
    m.points = scale_factor * m.points

    p_max = np.max(m.points, axis=0)
```

```
p_min = np.min(m.points, axis=0)

filename_split = mesh_filename.split("/")

filename_split[-1] = "scaled_" + filename_split[-1].split('.')[0] + '.gmsH'

new_filename = "/" .join(filename_split)
print(new_filename)

m.write(new_filename, file_format='gmsH')
```

# Appendix C

## Position of the Dipoles and Conversion of EEG positions

### C.1 Positions of the Dipoles

```
import bpy
ob = bpy.data.objects["whitematter"]
for v in ob.data.vertices:
    print(v.co.x, v.co.y, v.co.z)
```

### C.2 Conversion of EEG Positions

```
import sys
import meshio
import numpy as np

# reading subsampled mesh
m = meshio.read(sys.argv[1])

# reading original EEG positions
f = open(sys.argv[2], 'r')

# output file
fo = open(sys.argv[3], 'w')

outputlines = []
```

```
for line in f.readlines():
    l = line.split(",")
    p = np.array(l[1:4], dtype=np.float64)
    idx = np.argmin(np.linalg.norm(m.points - p,axis=1))
    new_p = m.points[idx]
    l[1:4] = [("%.16f" % pi) for pi in new_p]
    outputlines.append(",".join(l))

fo.writelines(outputlines)
```

# Bibliography

- [1] The University of Queensland. *Action potential and Synapses*. (visited on 14/05/2021). URL: <https://qbi.uq.edu.au/brain-basics/brain/brain-physiology/action-potentials-and-synapses> (cit. on p. 4).
- [2] The University of Queensland. *Lobes of the brain*. (visited on 20/05/2021). URL: <https://qbi.uq.edu.au/brain/brain-anatomy/lobes-brain> (cit. on pp. 4, 5).
- [3] Vijay P.B. Grover, Joshua M. Tognarelli, Mary M.E. Crossey, I. Jane Cox, Simon D. Taylor-Robinson, and Mark J.W. McPhail. «Magnetic Resonance Imaging: Principles and Techniques: Lessons for Clinicians». en. In: *Journal of Clinical and Experimental Hepatology* 5.3 (Sept. 2015), pp. 246–255. ISSN: 09736883. DOI: 10.1016/j.jceh.2015.08.001. URL: <https://linkinghub.elsevier.com/retrieve/pii/S0973688315004156> (visited on 12/04/2020) (cit. on p. 6).
- [4] Pedro Pallangyo, Frederick Lyimo, Paulina Nicholaus, Ulimbakisya Kain, and Mohamed Janabi. «Spontaneous Subdural Empyema Following a High-Parasitemia Falciparum Infection in a 58-Year-Old Female From a Malaria-Endemic Region: A Case Report». In: *Journal of Investigative Medicine High Impact Case Reports* 4 (July 2016), p. 2324709616666567. DOI: 10.1177/2324709616666567 (cit. on p. 7).
- [5] Hans Hallez et al. «Review on solving the forward problem in EEG source analysis». en. In: *Journal of NeuroEngineering and Rehabilitation* 4.1 (2007). Number: 1 Reporter: Journal of NeuroEngineering and Rehabilitation, p. 46. ISSN: 1743-0003. DOI: 10.1186/1743-0003-4-46. URL: <http://jneuroengrehab.biomedcentral.com/articles/10.1186/1743-0003-4-46> (visited on 08/21/2018) (cit. on pp. 7–10).
- [6] CD Binnie and PF Prior. «Electroencephalography.» In: *Journal of Neurology, Neurosurgery & Psychiatry* 57.11 (1994), pp. 1308–1319 (cit. on p. 8).

- [7] Christoph M. Michel, Micah M. Murray, Göran Lantz, Sara Gonzalez, Laurent Spinelli, and Rolando Grave de Peralta. «EEG source imaging». en. In: *Clinical Neurophysiology* 115.10 (Oct. 2004). Number: 10 Reporter: Clinical Neurophysiology, pp. 2195–2222. ISSN: 13882457. DOI: 10.1016/j.clinph.2004.06.001. URL: <http://linkinghub.elsevier.com/retrieve/pii/S1388245704002135> (visited on 08/21/2018) (cit. on p. 8).
- [8] Roberta Grech, Tracey Cassar, Joseph Muscat, Kenneth P Camilleri, Simon G Fabri, Michalis Zervakis, Petros Xanthopoulos, Vangelis Sakkalis, and Bart Vanrumste. «Review on solving the inverse problem in EEG source analysis». en. In: *Journal of NeuroEngineering and Rehabilitation* 5.1 (2008). Number: 1 Reporter: Journal of NeuroEngineering and Rehabilitation, p. 25. ISSN: 1743-0003. DOI: 10.1186/1743-0003-5-25. URL: <http://jneuroengrehab.biomedcentral.com/articles/10.1186/1743-0003-5-25> (visited on 08/21/2018) (cit. on pp. 10, 12).
- [9] Roberta Grech, Tracey Cassar, Joseph Muscat, Kenneth P Camilleri, Simon G Fabri, Michalis Zervakis, Petros Xanthopoulos, Vangelis Sakkalis, and Bart Vanrumste. «Review on solving the inverse problem in EEG source analysis». In: *Journal of neuroengineering and rehabilitation* 5.1 (2008), pp. 1–33 (cit. on p. 12).
- [10] Anirudh Vallabhaneni, Tao Wang, and Bin He. «Brain—computer interface». In: (2005), pp. 85–121 (cit. on p. 13).
- [11] Marcel Van Gerven et al. «The brain–computer interface cycle». In: *Journal of neural engineering* 6.4 (2009), p. 041001 (cit. on pp. 13–15).
- [12] Christophe Geuzaine and Jean-François Remacle. *A three-dimensional finite element mesh generator with built-in pre- and post-processing facilities*. URL: <https://gmsh.info/> (cit. on p. 20).
- [13] J. Rasgado-Toledo, F. Lizcano-Cortés, V. Olalde-Mathieu, M. Zamora-Ursulo, G. Licea-Haquet, A. Carillo-Peña, E. Navarrete, A.\* Reyes-Aguilar, and M Giordano. *"Pragmatic Language"*. 2021. DOI: 10.18112/openneuro.ds003481.v1.0.3 (cit. on pp. 25, 37).
- [14] Andy Jahn. *Andy's Brain Book*. URL: [https://andysbrainbook.readthedocs.io/en/latest/MRtrix/MRtrix\\_Introduction.html](https://andysbrainbook.readthedocs.io/en/latest/MRtrix/MRtrix_Introduction.html) (cit. on p. 27).
- [15] Zhao Qing and Gaolang Gong. «Size matters to function: Brain volume correlates with intrinsic brain activity across healthy individuals». In: *Neuroimage* 139 (2016), pp. 271–278 (cit. on pp. 38, 39).
- [16] HH Bartholomeusz, E Courchesne, and CM Karns. «Relationship between head circumference and brain volume in healthy normal toddlers, children, and adults». In: *Neuropediatrics* 33.05 (2002), pp. 239–241 (cit. on pp. 40, 41).

- [17] Liam M O'Brien et al. «Adjustment for whole brain and cranial size in volumetric brain studies: a review of common adjustment factors and statistical methods». In: *Harvard review of psychiatry* 14.3 (2006), pp. 141–151 (cit. on p. 42).